AD 729858

AFFDL-TR-71-58

STABILITY AND DRAG OF PARACHUTES WITH VARYING EFFECTIVE POROSITY

H. G. HEINRICH

E. L. HAAK

UNIVERSITY OF MINNESOTA

TECHNICAL REPORT AFFDL-TR-71-58

FEBRUARY 1971

AIR FORCE FLIGHT DYNAMICS LABORATORY
AIR FORCE SYSTEMS COMMAND
WRIGHT-PATTERSON AIR FORCE BASE, OHIO

76

NOTICE

When Government drawings, specifications, or other data are used for any purpose other than in connection with a definitely related Government procurement operation, the United States Government thereby incurs no responsibility nor any obligation whatsoever; and the fact that the government may have formulated, furnished, or in any way supplied the said drawings, specifications, or other data, is not to be regarded by implication or otherwise as in any manner licensing the holder or any other person or corporation, or conveying any rights or permission to manufacture, use, or sell any patented invention that may in any way be related thereto.

This report supersedes ASD-TDR-62-100, AD288572, same title, dated September 1962.

This document has been approved for public release and sale; its distribution is unlimited.

A

Copies of this report should not be returned unless return is required by security considerations, contractual obligations, or notice on a specific document.

AIR FORCE: 25-8-71/200

UNCLASSIFIED

Security Classification

DOCUMENT CONTROL DATA - R & D

(Security classification of title, body of abstract and indexing annotation must be entered when the overall report is classified)

1. ORIGINATING ACTIVITY (Corporate author): University of Minnesota, Minneapolis, Minnesota

2a. REPORT SECURITY CLASSIFICATION: Unclassified

2b. GROUP: N/A

3. REPORT TITLE: Stability and Drag of Parachutes with Varying Effective Porosity

4. DESCRIPTIVE NOTES (Type of report and inclusive dates): Final Report, June 1958 - June 1961

5. AUTHOR(S) (First name, middle initial, last name):
Heinrich, Helmut G.
Haak, Eugene L.

6. REPORT DATE: February 1971

7a. TOTAL NO. OF PAGES: 63

7b. NO. OF REFS: 8

8a. CONTRACT OR GRANT NO.: AF 33(616)-8310

b. PROJECT NO.: 6065

c.

d. Task 606503

9a. ORIGINATOR'S REPORT NUMBER(S): None

9b. OTHER REPORT NO(S) (Any other numbers that may be assigned this report): AFFDL-TR-71-58 (See Foreword)

10. DISTRIBUTION STATEMENT: This report has been approved for public release and sale; its distribution is unlimited.

11. SUPPLEMENTARY NOTES: None

12. SPONSORING MILITARY ACTIVITY: Air Force Flight Dynamics Laboratory, AFFDL (FER), Wright Patterson AFB, Ohio 45432

13. ABSTRACT

The tangent force, normal force, and moment coefficients versus the angle of attack of ten different types of parachutes have been determined by means of wind tunnel measurements. Models formed from sheet metal as well as made out of non-porous and porous cloth were used. The nominal porosity of the cloth varied from 10 to 275 ft^3/ft^2-min under a differential pressure of 1/2 inch of water. This corresponds to a range of effective porosity from 0.003 to 0.096.

The aerodynamic coefficients have been related to the effective and nominal porosity characteristics expressed as derivatives with respect to the porosity term.

It was found that the static stability of all types of parachutes could be significantly improved through higher porosity, although this reduces slightly the air resistance for the parachute.

DD FORM 1 NOV 65 1473

UNCLASSIFIED

Security Classification

UNCLASSIFIED
Security Classification

14 KEY WORDS	LINK A		LINK B		LINK C	
	ROLE	WT	ROLE	WT	ROLE	WT
Parachutes						
Effective Porosity						
Aerodynamic Coefficients						
Stability						
Drag						

UNCLASSIFIED
Security Classification

AFFDL-TR-71-58

FOREWORD

This report was originally published as ASD-TDR-62-100 with identical title. Subsequent to this publication, an error was discovered in the value of dynamic pressure used in calculating the force and moment coefficients. This report was prepared by the University of Minnesota and presents the revised data in a format identical to that used in ASD-TDR-62-100. (AD286570)

This report was submitted by the authors in December 1968.

This technical report has been reviewed and is approved.

GEORGE A. SOLT, Jr.
Chief, Recovery and Crew Station Br.
Air Force Flight Dynamics Laboratory

AFFDL-TR-71-58

STABILITY AND DRAG OF PARACHUTES WITH VARYING EFFECTIVE POROSITY

H. G. HEINRICH
AND
E. L. HAAK

Details of illustrations in
this document may be better
studied on microfiche

ABSTRACT

The tangent force, normal force, and moment coefficients versus the angle of attack of ten different types of parachutes have been determined by means of wind tunnel measurements. Models formed from sheet metal as well as made out of non-porous and porous cloth were used. The nominal porosity of the cloth varied from 10 to 275 ft^3/ft^2-min under a differential pressure of 1/2 inch of water. This corresponds to a range of effective porosity from 0.003 to 0.096.

The aerodynamic coefficients have been related to the effective and nominal porosity characteristics expressed as derivatives with respect to the porosity term.

It was found that the static stability of all types of parachutes could be significantly improved through higher porosity, although this reduces slightly the air resistance of the parachute.

TABLE OF CONTENTS

LIST OF ILLUSTRATIONS

LIST OF TABLES

LIST OF SYMBOLS

b	=	Nominal porosity
C	=	Effective porosity
C_D	=	Drag coefficient
C_M	=	Pitching moment coefficient ("moment coefficient")
C_N	=	Normal force coefficient
C_T	=	Tangent force coefficient
D_d	=	Design diameter
D_o	=	Nominal diameter
D_p	=	Projected or in-flight diameter
d	=	Total inflated model length
h	=	Inflated canopy depth
k	=	Moment arm
l	=	Suspension line length
M	=	Pitchimg moment ("moment")
N	=	Normal force
q	=	Dynamic pressure = $\frac{1}{2}\rho V^2$
S_d	=	Canopy area based on D_d
S_o	=	Canopy area based on D_o
S_p	=	Canopy area based on D_p
T	=	Tangent force
V	=	Velocity
α	=	Angle of attack
ρ	=	Air density

SUBSCRIPTS

d	=	Based on design diameter
o	=	Based on nominal diameter
p	=	Based on projected diameter

SECTION I

INTRODUCTION

The performance characteristics of most conventional parachutes, and their range and mode of variation, are fairly well known. One of the most interesting aspects of parachute performance is its dependence on the air permeability of the parachute material under the particular operating conditions. The air permeability of the cloth is a function of the Reynolds and Mach numbers under which the parachute has to function. These relationships have been subject to special investigations, as, for example, reported in Ref 1, Section 4.

The aerodynamic characteristics of any parachute made out of porous material depend strongly on the effective porosity, and since its performance is governed by the aerodynamic characteristics, one may state that each type of parachute functions to a large extent in accordance with its effective porosity. Therefore in the following chapters an attempt is made to present the aerodynamic parameters of ten conventional parachute types as functions of effective porosity.

Since the effective porosity can be calculated for a wide range of conditions (Ref 1), the parameters presented in this report can be used for the calculation of the rate of descent and for an approximate determination of static stability features and dynamic stability behavior depending on the altitude and velocity at which the parachute functions.

SECTION II
EXPERIMENTS

2.1 Coordinate System and Coefficients

In this study the physical coordinates of the parachute are used as the major axes (Fig 1). For this case, the following forces and moments are encountered:

a) The tangent force, T, acting along the centerline of the parachute. This is a drag force at zero angle of attack.

b) The normal force, N, acting perpendicular to the parachute centerline.

c) The moment, M, defined as the aerodynamic moment about the nominal confluence point of the parachute suspension lines. The moment is positive when in the same direction as the angle of attack and is stabilizing when the slope $dC_M/d\alpha$ is less than 0 (Ref 2).

The force and moment coefficients were calculated from test data and employed the conventional aerodynamic relationships (Ref 2), where

$$C_T = \frac{T}{qS} , \tag{1}$$

$$C_N = \frac{N}{qS} , \tag{2}$$

and

$$C_M = \frac{M}{qSD} . \tag{3}$$

Equations 1 and 2 use direct force readings from the wind tunnel balance system. In the general case, we see from Fig 1A that

$$N = N_1 + N_2 \tag{4}$$

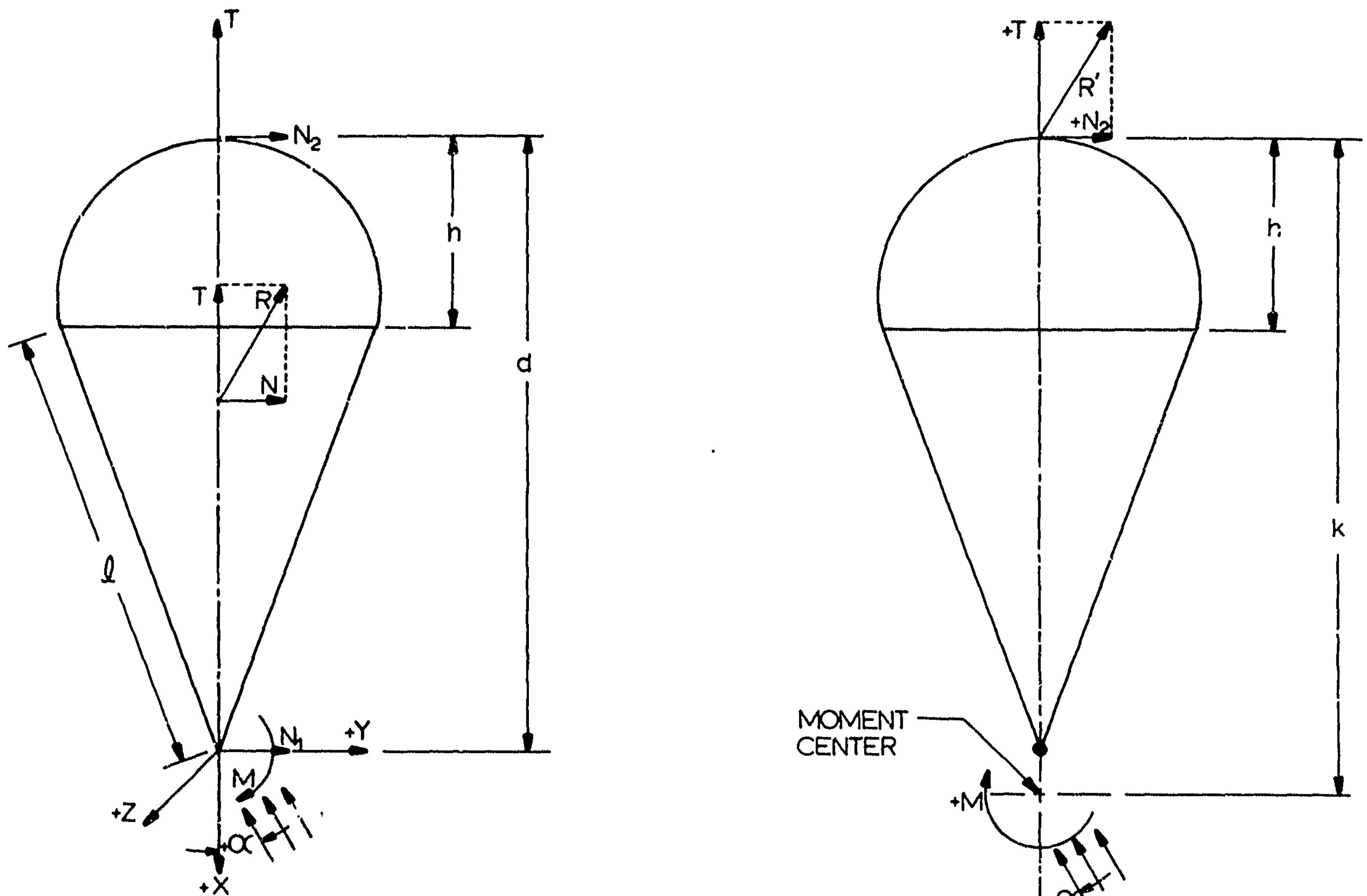

A). GENERAL SYSTEM

B). WIND TUNNEL SYSTEM (NEGLECTING N_1)

FIG. 1. PARACHUTE COORDINATE SYSTEM AND FORCES

and

$$M = N_2 \cdot d \quad . \tag{5}$$

However, the measurements indicated that over a wide range of angle of attack

$$N_1 << N_2 \tag{6}$$

and in the following evaluation N_1 has been neglected. A similar experience was reported in Ref 3. Then from Fig 1B we see that

$$N = N_2 \tag{4a}$$

and

$$M = N_2 \cdot k \quad . \tag{5a}$$

By convention, the nominal diameter is used for all calculations where more or less conventional flat design parachutes were used, and the area "S" and length "D" above were based on this diameter D_o (Ref 2). In the cases of the ribbed and ribless guide surface parachutes where it is impractical to define a "nominal" diameter, the construction diameter, D_d, and its related circular area were used (Ref 2), while the characteristic length, "D", above was adjusted to 1.33 D_d.

2.2 Models

Parachute models were fabricated from rigid non-porous metal, flexible non-porous polyethylene, and from flexible porous textile materials. Including the formed metal and polyethylene models, a total of 45 parachute models were studied.

The ten types of parachute canopies were:

1) Circular flat
2) 10% flat extended skirt
3) 14.3% full extended skirt

4) Personnel guide surface

5) Conical - 28 gores circular flat with 4 gores removed

6) Ribless guide surface

7) Ribless guide surface with spoilers

8) Ribbed guide surface stabilization type

9) Ribbon

10) Ringslot

Gore patterns and design details for these parachute types are given in Ref 2.

To obtain in-flight shapes for the formed metal models, a number of dimensionless profiles were obtained from Ref 4 and other publications. Details of these profiles are shown in Appendix B of this report. The flexible polyethylene models were constructed from the same gore patterns as the textile models.

The nominal diameter D_o of all rigid and flexible circular flat type parachute models was in the order of 16 inches. The ribbed and ribless guide surface parachutes had design diameters D_d of 12 inches and 12.6 inches respectively. All solid cloth circular flat type parachutes had 28 gores and 28 suspension lines. Significant dimensions of all models are given in Table A-1, Appendix A.

The suspension lines used on all flexible models were nylon core cord, MIL-C-5040B, with a 0.096 inch diameter. In order to establish the effect of these rather thick suspension lines on the aerodynamic coefficients, a limited number of wind tunnel studies were made using much thinner suspension lines. This study is described in Appendix C; results show that the effect of the suspension line diameter on the measured forces is negligible.

The textile models were made from nylon cloth varying in porosity from 10 to 275 ft^3/ft^2-min under a differential pressure of 1/2 inch of water or over a range of effective porosity from 0.003 to 0.096.

All the rigid metal models were fabricated from 1/16 inch aluminum or copper with four 1/8 inch steel wires used as suspension lines.

Figure 2 shows the rigid, polyethylene and textile models of the 10% flat extended skirt parachute mounted in the wind tunnel.

2.3 Test Arrangement and Procedure

A horizontal return, atmospheric pressure wind tunnel with a test section of 38 x 54 inches was used to conduct these experiments. The models were suspended in a plate turntable as illustrated in Figs 3 and 4.

Initial tests indicated that upstream disturbances influenced significantly the basic stability parameters of the parachute canopy, and it became necessary to make the frontal area of the suspension system as small as possible and to arrange all of the balance components downstream of the model. Appendix D describes these disturbance effects and the modifications made in the test setup to remove them. As seen in Fig 4, the normal force sensing element was mounted near the apex of the parachute between the model and the sting. The tangent force pick-up was mounted between the strut in the rear of the test section and the centerline sting. Both sensing elements incorporate standard strain gage circuits mounted on elastic cantilever beams. The strain gage balances are shown in Figs 5 and 6.

The wind tunnel Mach number was M = 0.1 for most of the tests, yielding a Reynolds number of approximately 6×10^5. In a few instances, strong model vibrations required a speed reduction, thus lowering the Reynolds number to approximately 4×10^5. Appropriate Reynolds numbers are given later, together with the graphical presentation of the results.

In conducting the tests, the turntable was set to the highest positive angle of attack which would still allow

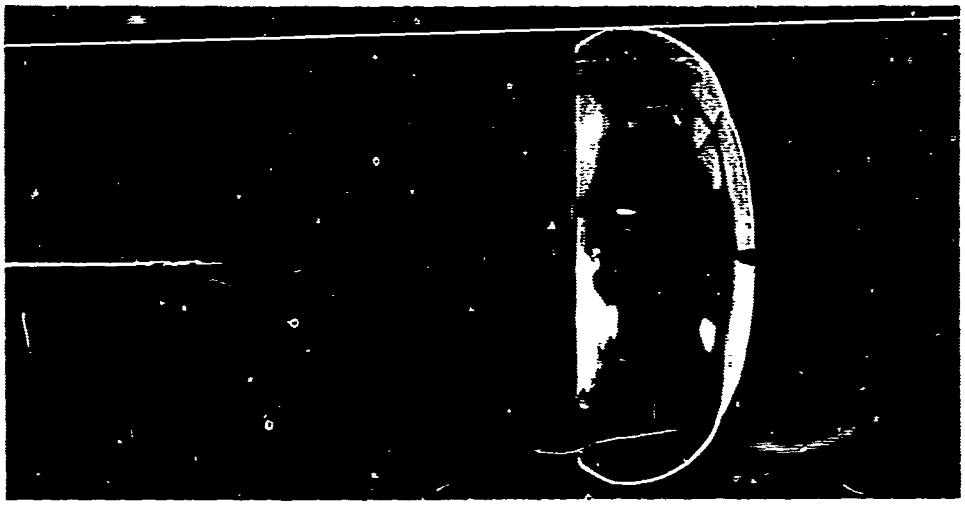

A. RIGID MODEL

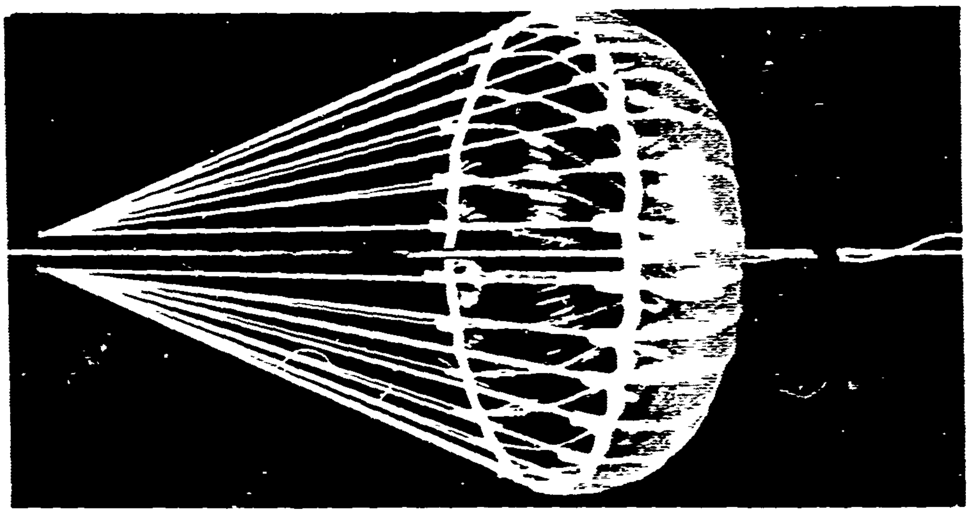

B. POLYETHYLENE MODEL

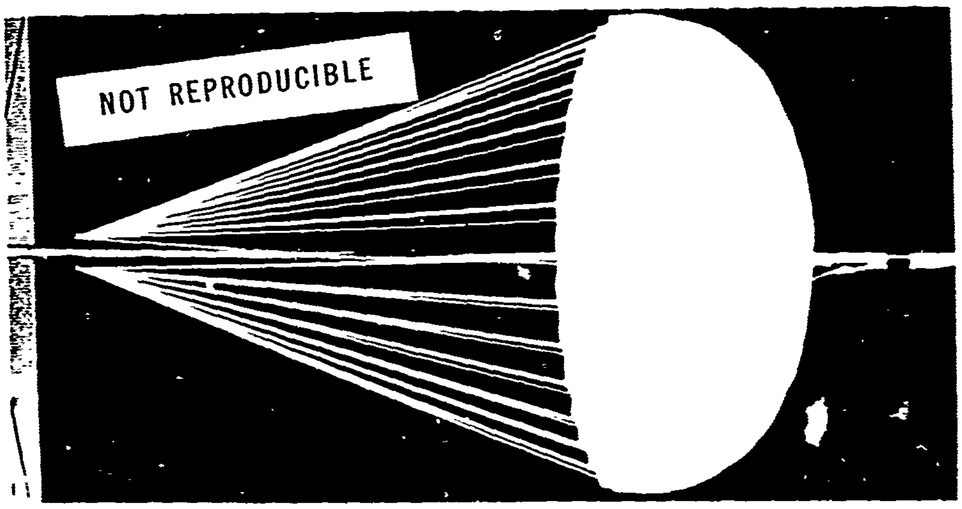

C. TEXTILE MODEL

FIG 2. MODELS OF A 10% FLAT EXTENDED SKIRT PARACHUTE IN WIND TUNNEL

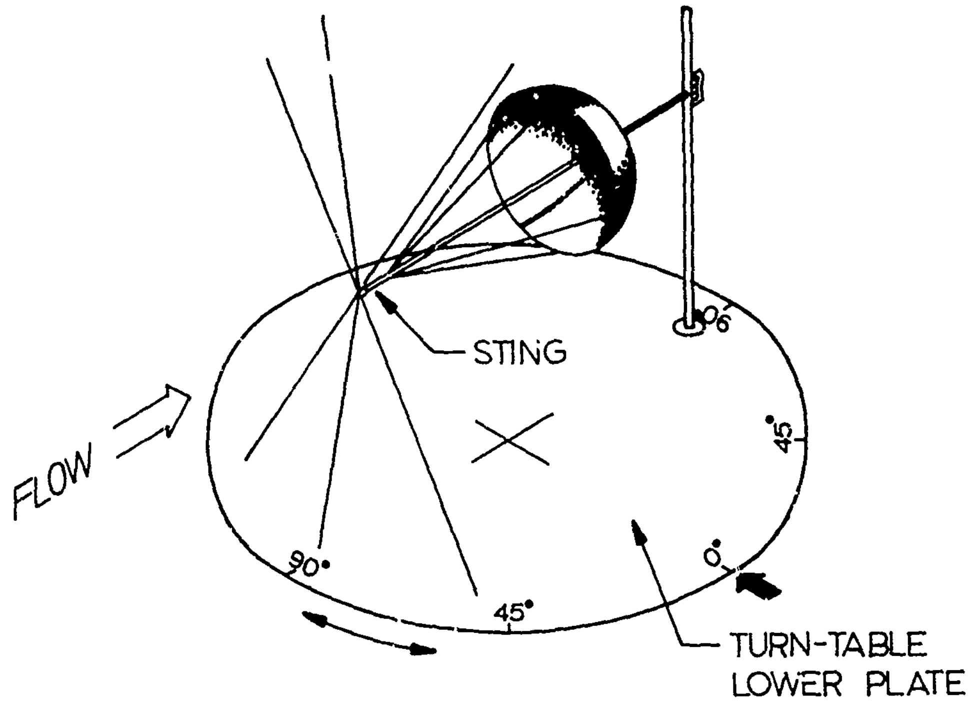

FIG 3. MODEL SUSPENSION

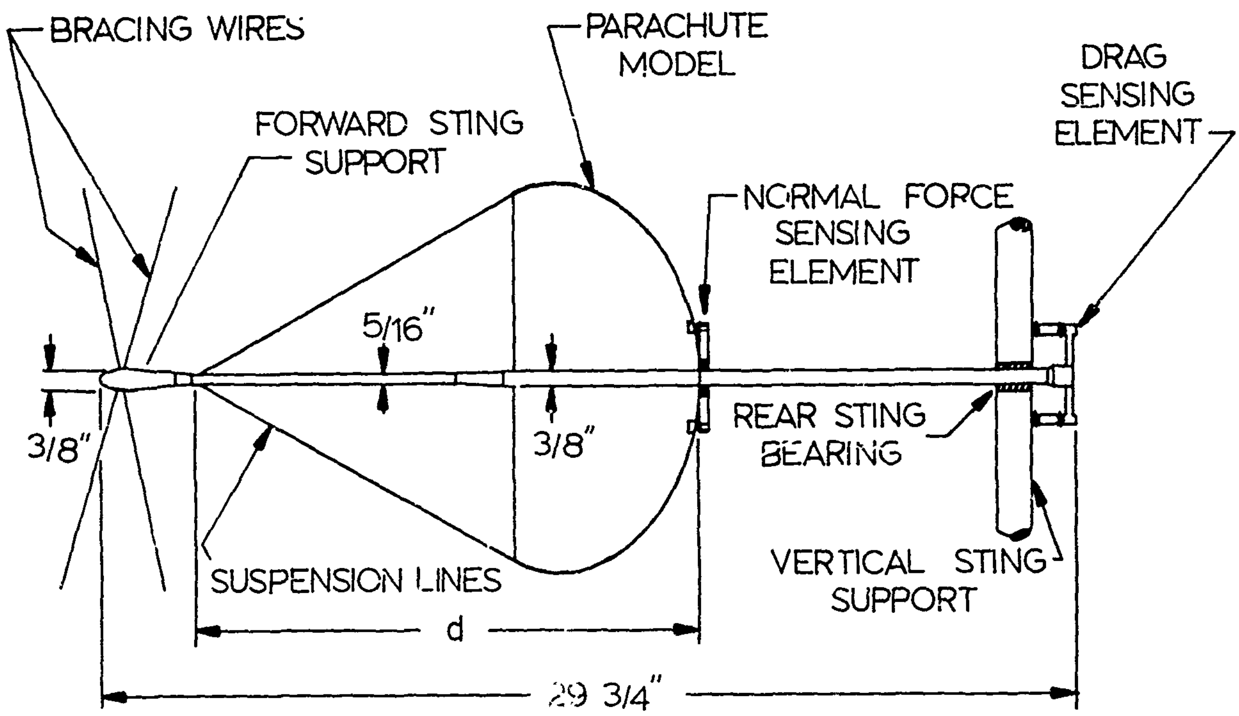

FIG 4. MODEL SUSPENSION AND STRAIN GAGE BALANCE ARRANGEMENT

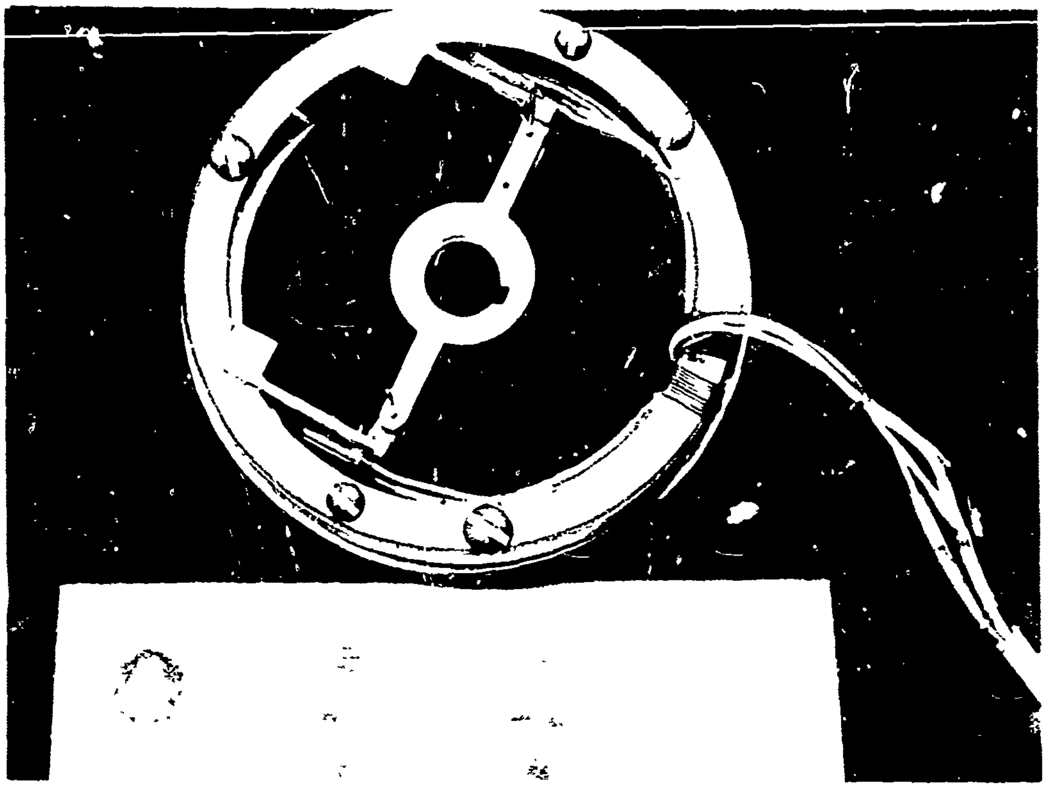

FIG 5. NORMAL FORCE SENSING ELEMENT

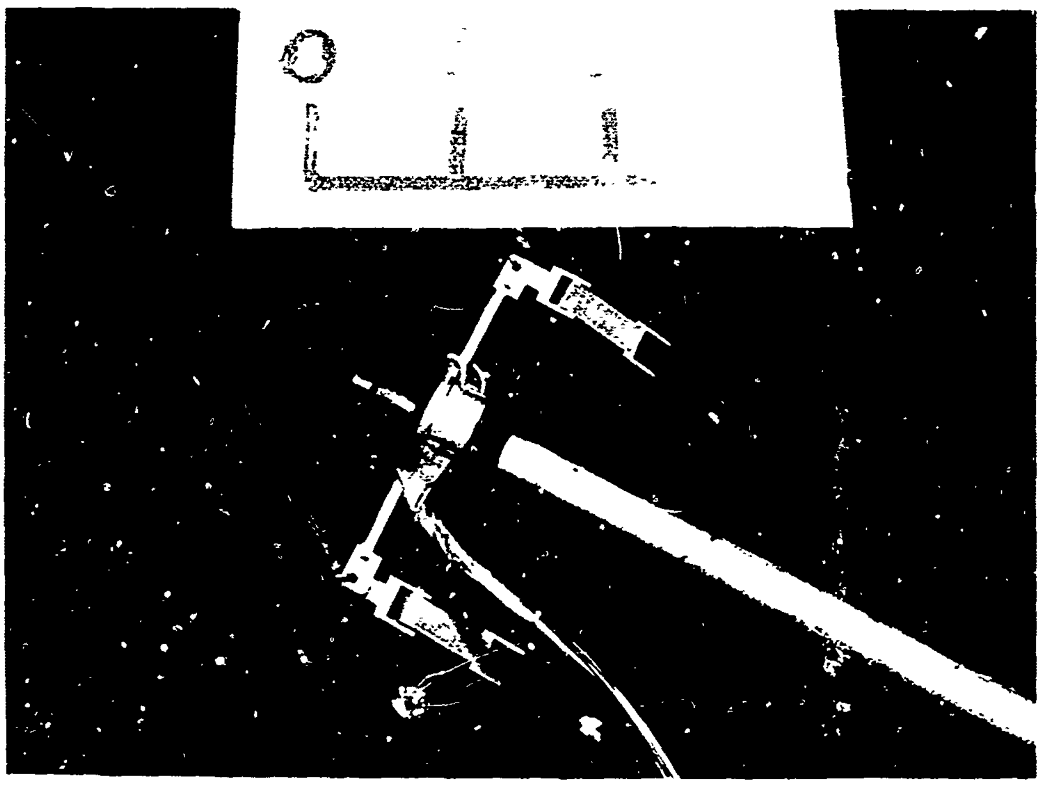

FIG 6. TANGENT FORCE SENSING ELEMENT

proper inflation of the textile parachute and a force recording was accomplished by means of a Century amplifier and recording oscillograph. The angle of attack was then successively reduced by five degree increments and the forces were recorded. To insure adequate accuracy at the smaller angles of attack, force measurements were taken in increments of $2\frac{1}{2}$ degrees. The turntable was rotated in this manner to the highest negative angle of attack and then returned in the same stepwise way to the starting point. This process was repeated four times in order to assure satisfactory accuracy of the recordings. The balance systems were statically calibrated at the beginning and end of the test.

From the oscillograph recordings, the aerodynamic coefficients were derived as described above, and all results are presented in detail in Appendix A of this report. To ascertain the repeatability of the test system, a number of the parachute models were again tested at a later date, and it was found that the coefficients deviated less than two per cent from the original data.

SECTION III
THE CONCEPT OF EFFECTIVE POROSITY*

The porosity, also called air permeability, of parachute cloth is conventionally expressed as the volumetric flow rate of air through a unit area of cloth at a specified differential pressure (usually 1/2 inch H_2O and at sea level conditions).

For aerodynamic and dynamic considerations, a dimensionless term, which relates a fictitious but physically conceivable free stream velocity "V" and an assumed average velocity "U" through the total area of the porous sheet, is

*Abstract from Reference 1

preferable. Figure 7 shows schematically the cloth as a grid in free air flow and the derivation of this dimensionless term.

This ratio, U/V, is called the effective porosity of the cloth, and has been established for a number of parachute materials (Ref 1). Figure 8 shows the effective porosity of 40# nylon cloth (nominal porosity = 120 ft^3/ft^2-min) versus the density ratio σ. From this graph it can be seen that effective porosity decreases with decreasing density and with increasing differential pressure ratio.

The possible consequences of the change of effective porosity, in particular, its decline with air density, on the drag and stability of parachutes is quite apparent. Therefore, the effective porosity has been utilized as a parameter wherever possible throughout this report. A formula which can be used to convert nominal porosity (ft^3/ft^2-min at 1/2 inch H_2O differential pressure) into effective porosity is given in Appendix A. Figure 9 presents effective porosity of cloths used for several models of varying nominal porosity as a function of differential pressure at sea level.

In order to determine the effect of cloth porosity on the drag and stability coefficients of the various parachutes, models were fabricated from three different materials (non-porous rigid metal, non-porous flexible polyethylene, and porous flexible cloth). From these three types of models, the dependency of the aerodynamic coefficients upon the porosity was readily apparent. It should be pointed out, however, that the differences observed between the non-porous metal models and the non-porous flexible models also include the effect of a difference in the basic shape of the canopies.

The variation of the aerodynamic parameters among the flexible models of different porosities can be understood as being primarily the effect of the porosity variation.

All flexible models which have been measured are listed in Table 1.

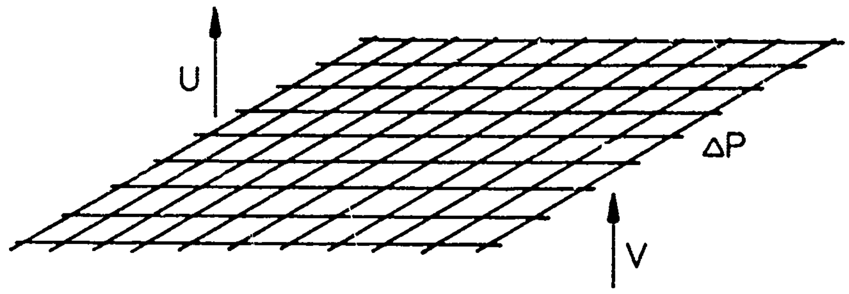

EFFECTIVE POROSITY $C=\frac{U}{V}$

WITH $\Delta P=\frac{\rho}{2}V^2$, $C=\frac{U}{\sqrt{\frac{2\,\Delta P}{\rho}}}$

FIG 7 DERIVATION OF THE TERM "EFFECTIVE POROSITY" (REF. 1)

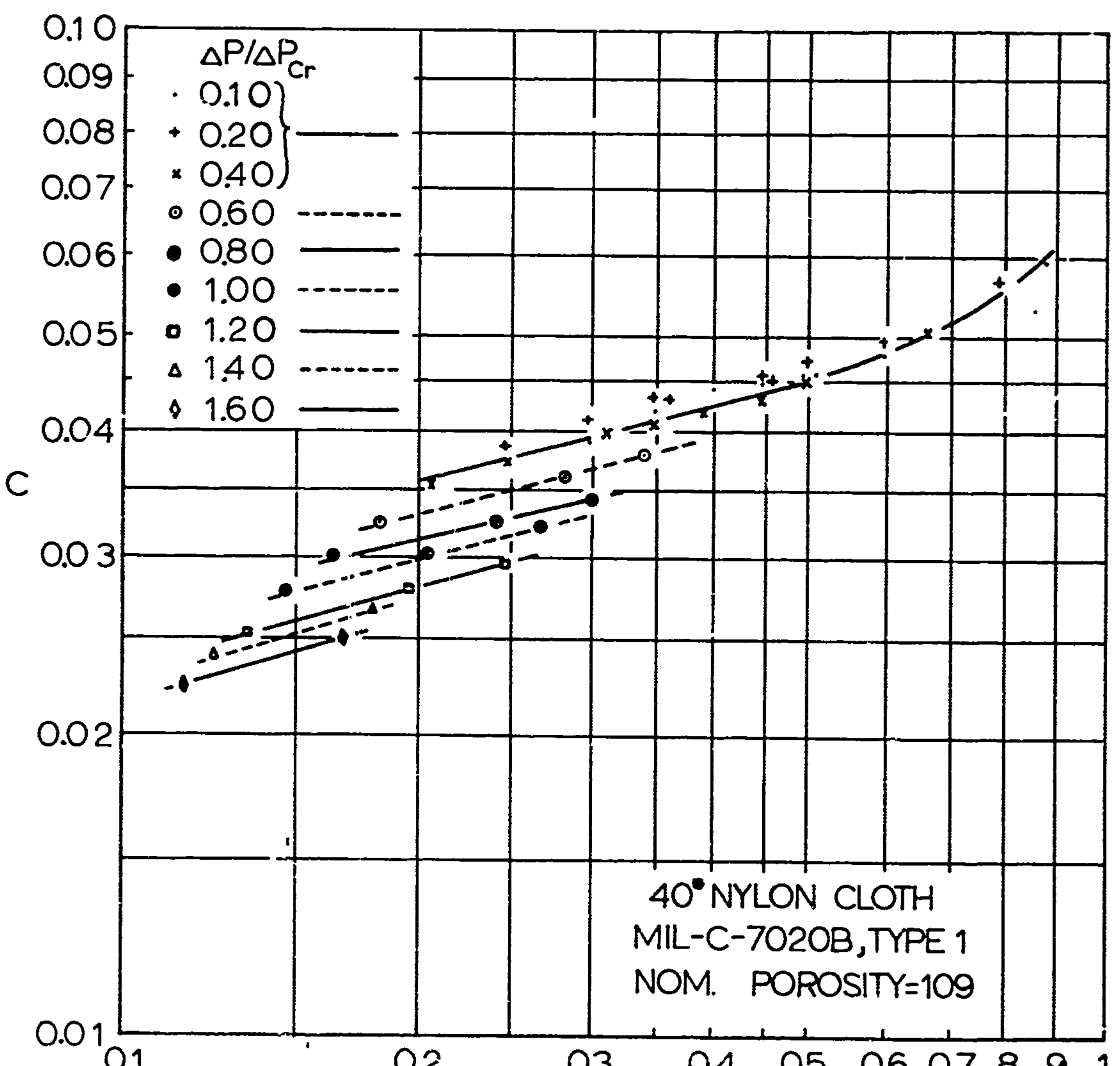

FIG 8. EFFECTIVE POROSITY VERSUS DENSITY RATIO (REF. 1)

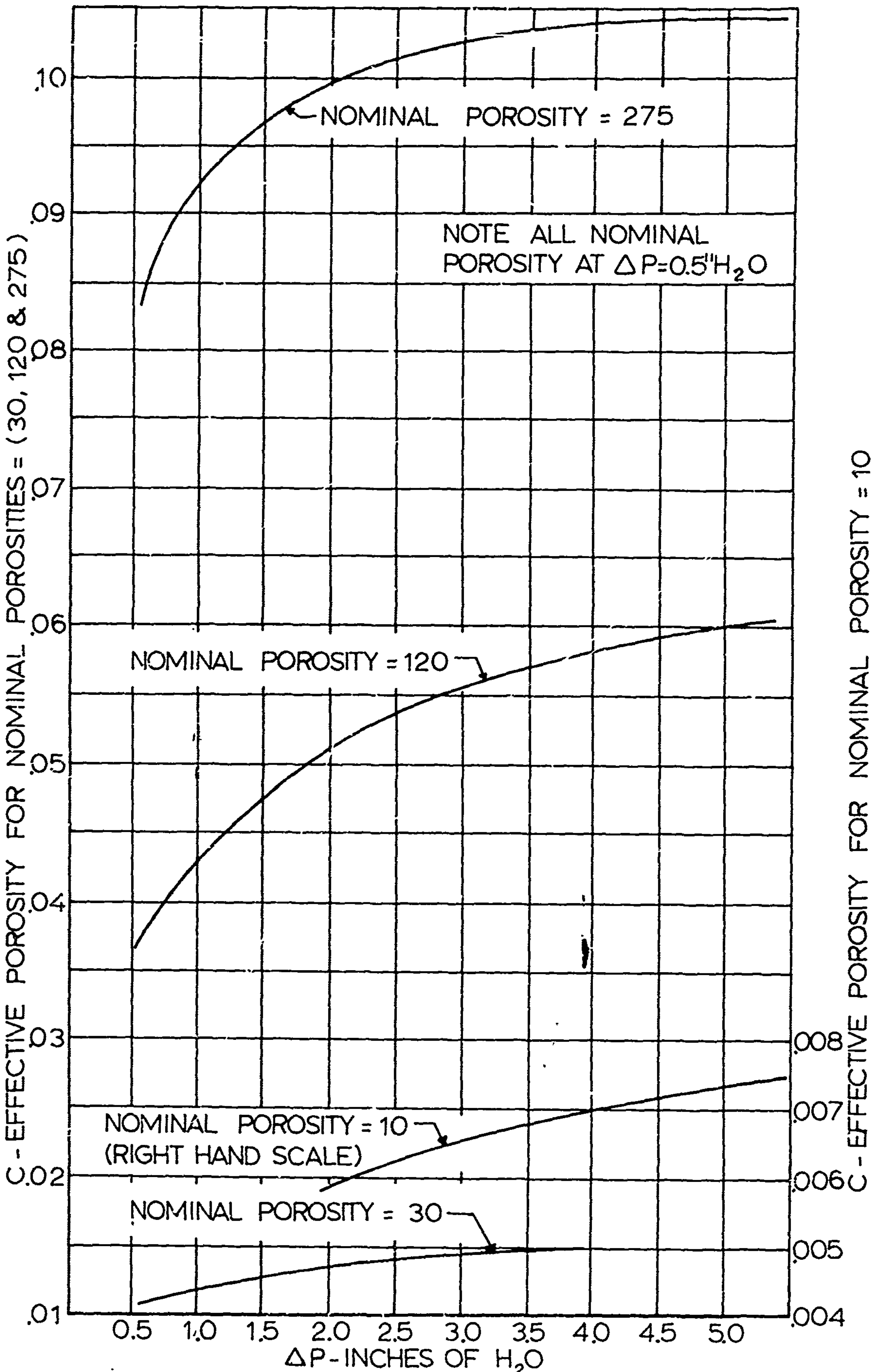

FIG 9. EFFECTIVE POROSITY OF VARIOUS CLOTHS

PARACHUTE TYPE	POROSITY AT 1/2 IN H_2O		GEOMETRIC POROSITY, %
	NOMINAL POROSITY, FT^3/FT^2-MIN	EFFECTIVE POROSITY, C	
Circular Flat	0, 10, 30, 120, and 275	0, .003, .010, .042, and .096	- - - - -
14.3 Full Extended Skirt	10 and 120	.003 and .042	- - - - -
10% Flat Extended Skirt	0, 10, 30, 120, and 275	0, .003, .010, .042, and .096	- - - - -
Conical	30 and 120	.010 and .042	- - - - -
Personnel Guide Surface	120 and 275	.042 and .096	- - - - -
Ribless Guide Surface	0, 10, 30, 120, and 275	0, .003, .010, .042, and .096	- - - - -
Ribless Guide Surface with Spoilers	30 and 120	.010 and .042	- - - - -
Ribbed Guide Surface	30 and 120	.010 and .042	- - - - -
Ribbon, 50" Prototype	- - - - - - - - - - - -	- - - - - - - - - - - -	20 and 30
Ribbon, 100" Prototype	- - - - - - - - - - - -	- - - - - - - - - - - -	20
Ring Slot, 50" Prototype	- - - - - - - - - - - -	- - - - - - - - - - - -	20 and 30
Ring Slot, 100" Prototype	- - - - - - - - - - - -	- - - - - - - - - - - -	20

TABLE 1. FLEXIBLE PARACHUTE MODELS UNDER CONSIDERATION

SECTION IV
RESULTS AND ANALYSIS

The magnitude of the vertical velocity of a descending parachute at a given air density depends on the coefficient of the tangent force at that particular angle of attack at which the tangent force coincides with the force vector of the suspended weight (Ref 5). This condition is satisfied when the normal force diminishes to zero. In order to maintain such a position it is necessary that at this particular point the moment characteristic of the parachute is such that it develops a restoring moment against any deflection of the parachute from this particular angle of attack. In view of the definitions shown in Fig 1, the slope of the moment curve must be negative, $dC_M/d\alpha < 0$, in order to satisfy this condition. The angle at which $C_N = 0$ and $dC_M/d\alpha < 0$ is called the stable angle of attack, α_{stable}.

The derivative of the moment curve is also a significant parameter in the study of the dynamic stability of the parachute, and the question of whether or not a parachute ever attains this position is a complicated dynamic problem. This is particularly true for parachutes whose stable angle of attack differs from zero. Practice shows that these parachutes may attain a gliding motion without much oscillation or they may oscillate, sometimes violently, within their range of instability. Because of dynamic effects they also may overshoot this range considerably (Ref 5).

The results of the measurements on all parachutes under investigation are shown in Appendix A. An inspection of the graphs shows that for moderate porosities, only the guide surface, ribbon, and ringslot parachutes are statically stable at zero angle of attack ($\alpha_{stable} = 0$). For these parachutes then, the aerodynamic coefficients at zero angle of attack are significant for performance calculations, and excluding other effects such as structural failure, partial inflation, etc., one may expect a motion free of oscillations with a well defined rate of descent.

Many graphs indicate a variation of the stable angle of attack with porosity. This is true for all parachutes, including ribbon and ringslot parachutes. However, ribbon and ringslot parachutes are built with geometric or inherent porosity, while the solid cloth parachutes are made of porous textile sheets which change their air permeability depending on Mach and Reynolds numbers as shown in the investigation concerning effective porosity. Ribbon grids will also change their effective porosity; however, it appears that those changes will be much smaller than the changes for cloth, at least in the region of incompressible flow.

In view of the relationship between effective porosity and the aerodynamic characteristics, the results of the experiments shall be discussed on the basis of the effective porosity applicable to the particular test conditions. In this respect, Table 2 shows a summary of data which is considered to be most significant for practical applications.

An inspection of Table 2 indicates that the effective drag coefficients, $C_{T_{\alpha\,stable}}$, (Ref 5) are generally in agreement with those determined by full size drop tests and slightly lower than the data of Ref 6, which was obtained from drop tests of models in a large hangar. Any discrepancies in all of the above data may partially arise from the fact that in one group of experiments all conditions are well known and the parachute models may also be at least partially restrained, whereas in free drop tests uncontrolled conditions may exist. For practical applications, it is suggested to base calculations of the rate of descent on data provided in Ref 2, but to adopt the information contained in this report for considerations related to the stability characteristics (α_{stable}, $dC_M/d\alpha$) and to predict the changes of the effective drag and stability induced through the variation of the effective porosity.

PARACHUTE TYPE	Porosity at $\frac{1}{2}$" H_2O		$C_{D_{\alpha}} = 0$	α_{stable}	$\left[\frac{dC_M}{d\alpha}\right]_{\alpha=0}$ deg^{-1}	$\left[\frac{dC_M}{d\alpha}\right]_{\alpha_{stable}}$ deg^{-1}	$C_{T_{\alpha_{stable}}}$
	Nominal	Effective					
Circular Flat	120	0.0419	0.684	19.8°	+0.0044	-0.0026	0.694
10% Flat Extended Skirt	120	0.0419	0.629	20.5°	+0.0044	-0.0041	0.634
Conical	120	0.0419	0.720	21.7°	+0.0040	-0.0040	0.739
Personnel Guide Surface	120	0.0419	0.790	5.4°	+0.0012	-0.0010	0.788
Ribless Guide Surface	30	-0.0105	0.788	0°	-0.0120	-0.0120	0.788
Ribbed Guide Surface	30	0.0105	0.882	0°	-0.0200	-0.0200	0.882
50" Prototype Ribbon		20% Geo.	0.548	0°	-0.0052	-0.0052	0.548
100" Prototype Ribbon		20% Geo.	0.574	0°	-0.0068	-0.0068	0.574
100" Prototype Ring Slot		20% Geo.	0.594	0°	-0.0040	-0.0040	0.594

TABLE 2. AERODYNAMIC COEFFICIENTS OF FARACHUTES WITH VARIOUS NOMINAL POROSITIES

Turning now to the results obtained with the solid cloth parachutes, Figs 10 through 12 show the characteristics of the circular flat, 10% flat extended skirt, and personnel guide surface parachute models expressed in the form of the tangent force, normal force, and moment coefficients versus angle of attack with cloth porosity as parameter. It can be seen that by increasing the cloth porosity, the angle of attack at which the parachute is statically stable will be reduced. For these three parachutes, there seems to exist an almost linear relationship between the effective porosity and the stable angle of attack, as shown in Fig 13.

Associated with the increase in effective porosity is a general decrease of the tangent force coefficient at the stable angle of attack, $C_{T_{\alpha stable}}$, as illustrated in Fig 14. It is interesting to note that for an effective porosity which is high enough to cause for all three parachutes static stability at $\alpha = 0$, the drag coefficient of the three quite different parachutes appear to be converging to approximately the same value.

Since an increase in effective porosity denotes, in principle, an increased air flow through the parachute cloth, one would intuitively expect in all cases a decrease in tangent force. However, the ribless and ribbed guide surface parachutes show an increase in tangent force with increasing cloth porosity through a considerable porosity range (Fig 15). Although this phenomenon has not been thoroughly studied, it appears that the increase in drag coefficient with porosity is caused by a change of shape of the canopy. The airflow through a low porosity parachute is small, and the internal pressure in the canopy is nearly equal to the stagnation pressure while the pressure on the outside of the guide surface is somewhat lower. This causes the guide surfaces of the canopy to bulge out into the flow. When the porosity is increased, the internal pressure decreases slightly but the pressure acting upon the guide surfaces remains essentially unchanged, which leads ultimately

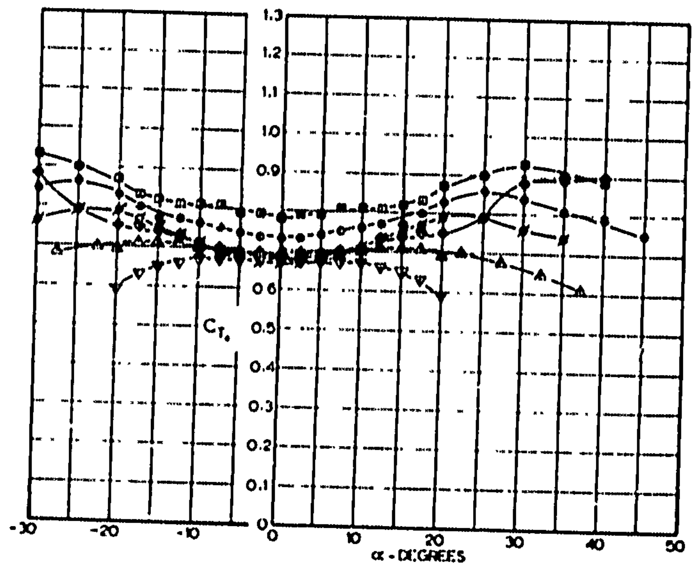

CIRCULAR FLAT

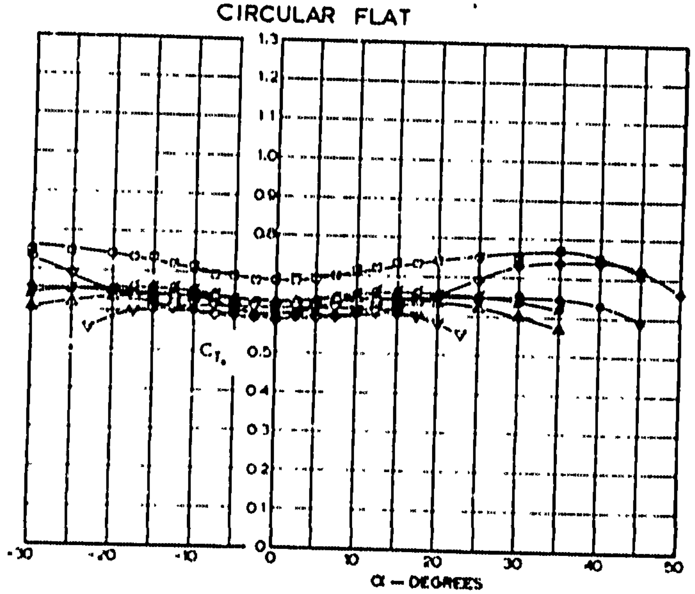

10% EXTENDED SKIRT

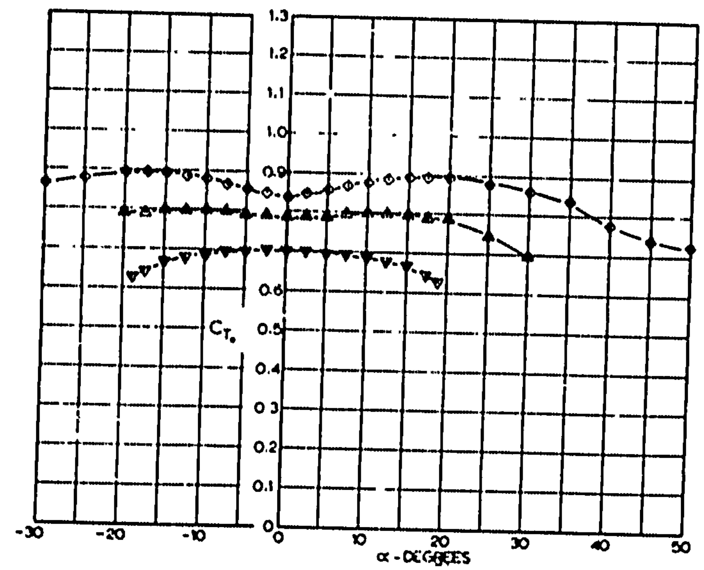

PERSONNEL GUIDE SURFACE

SYMBOL	NOMINAL POROSITY (FT^3/FT^2-MIN)	EFFECTIVE POROSITY
▽	275	0096
△	120	0042
#	30	0010
○	10	0003
◇	0	00 (RIGID)
□	0	00 (POLY)

FIG 10. TANGENT FORCE COEFFICIENT VERSUS ANGLE OF ATTACK OF VARIOUS PARACHUTES

BASED ON TOTAL CLOTH AREA

REYNOLDS NO ≈ 6×10^5

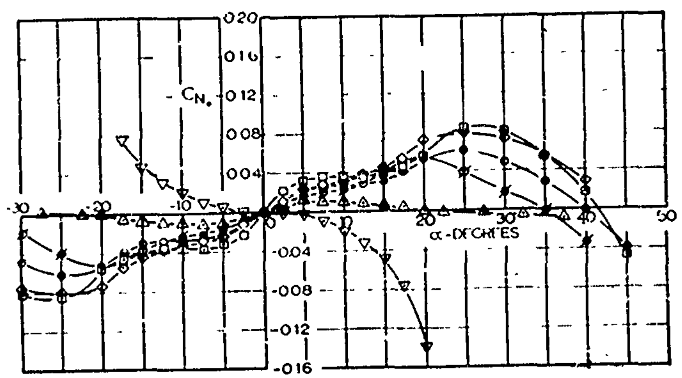

CIRCULAR FLAT

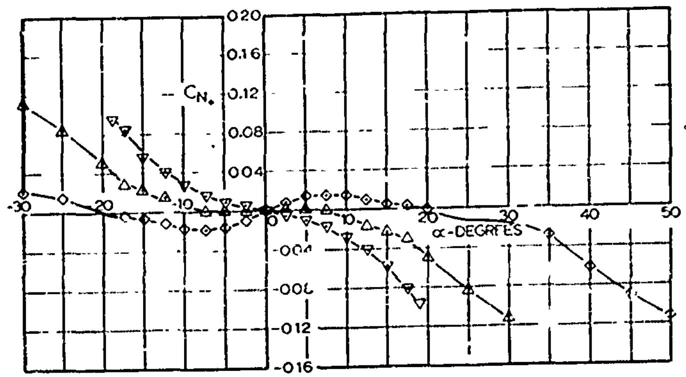

PERSONNEL GUIDE SURFACE

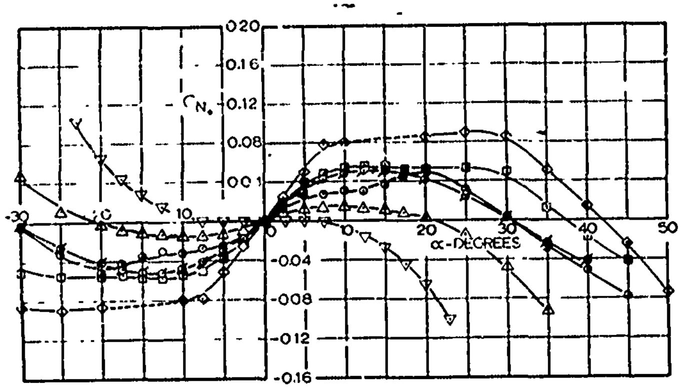

10% EXTENDED SKIRT

SYMBOL	NOMINAL POROSITY (FT³/FT²-MIN)	EFFECTIVE POROSITY
▽	275	0096
△	120	0042
ø	30	0010
○	10	C003
◇	0	CC (RIGID)
□	0	CO (POLY)

FIG 11 NORMAL FORCE COEFFICIENT VERSUS ANGLE OF ATTACK OF VARIOUS PARACHUTES

BASED ON TOTAL CLOTH AREA

REYNOLDS NO. ≈ 6×10^5

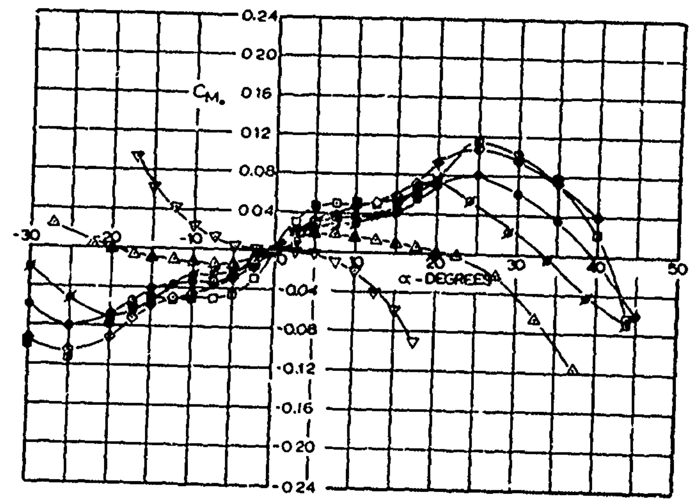

CIRCULAR FLAT

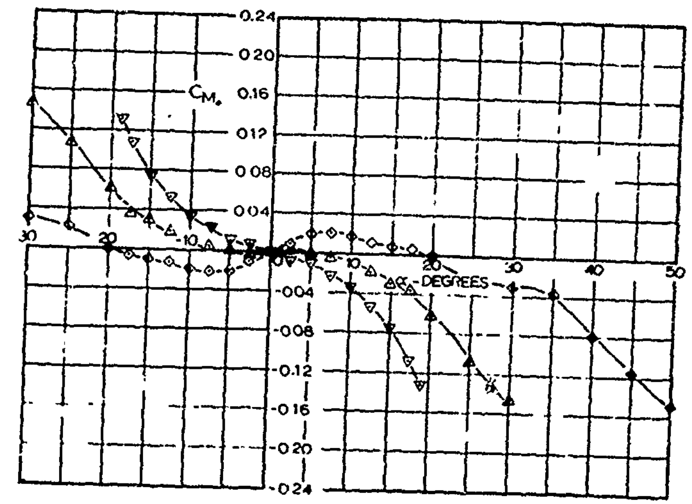

PERSONNEL GUIDE SURFACE

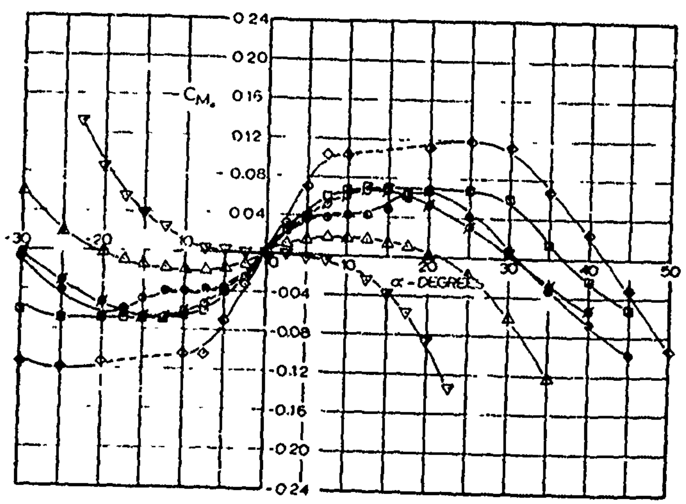

10 % EXTENDED SKIRT

SYMBOL	NOMINAL POROSITY (FT^3/FT^2 - MIN)	EFFECTIVE POROSITY
▽	275	0096
△	120	0042
▲	30	0010
○	10	0003
◇	0	00 (RIGID)
□	0	00 (POLY)

FIG 12 MOMENT COEFFICIENT VERSUS ANGLE OF ATTACK OF VARIOUS PARACHUTES

BASED ON TOTAL CLOTH AREA

REYNOLDS NO = 6×10^5

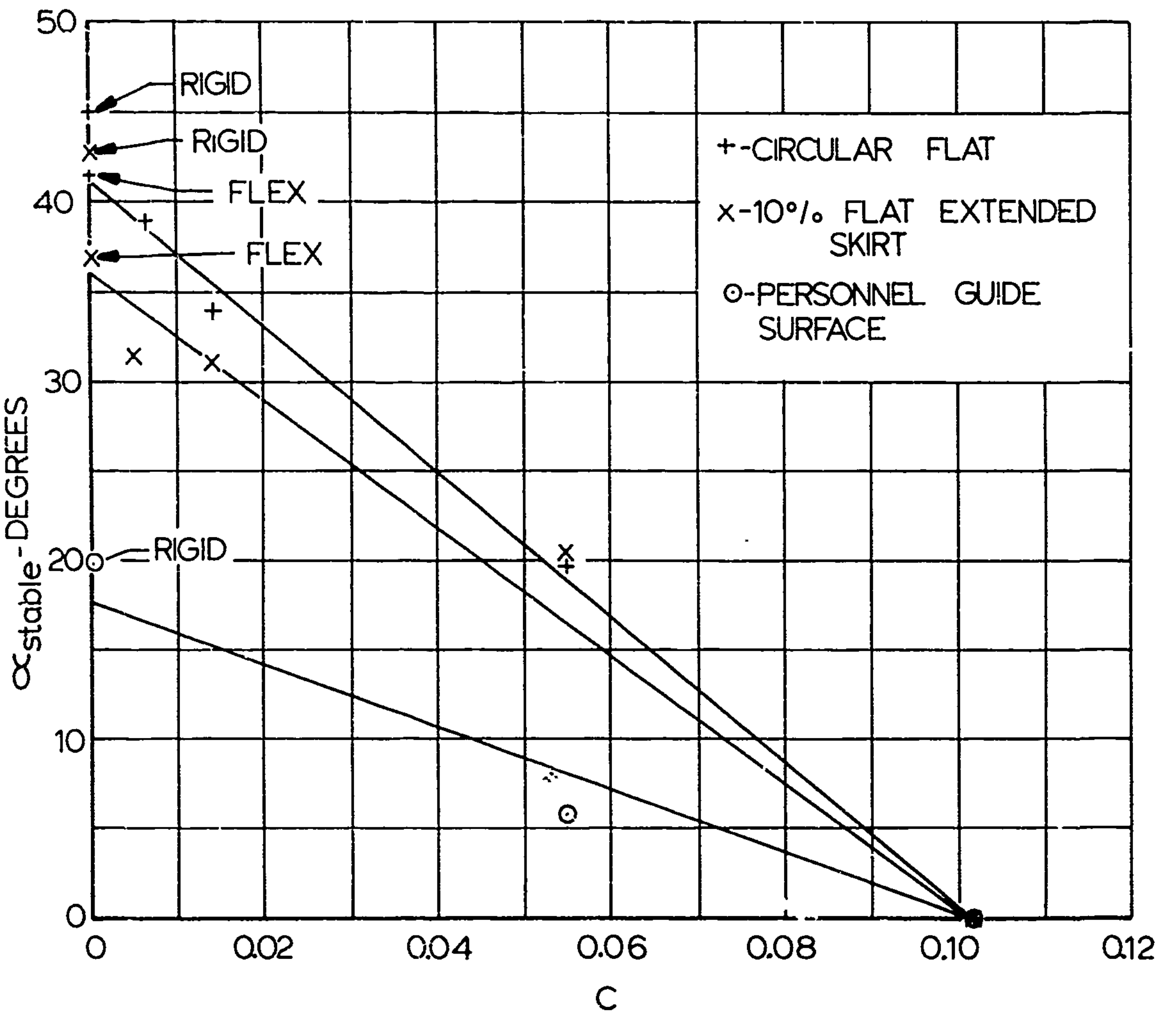

FIG 13. STABLE ANGLE OF ATTACK AS A FUNCTION OF EFFECTIVE POROSITY FOR SEVERAL PARACHUTES

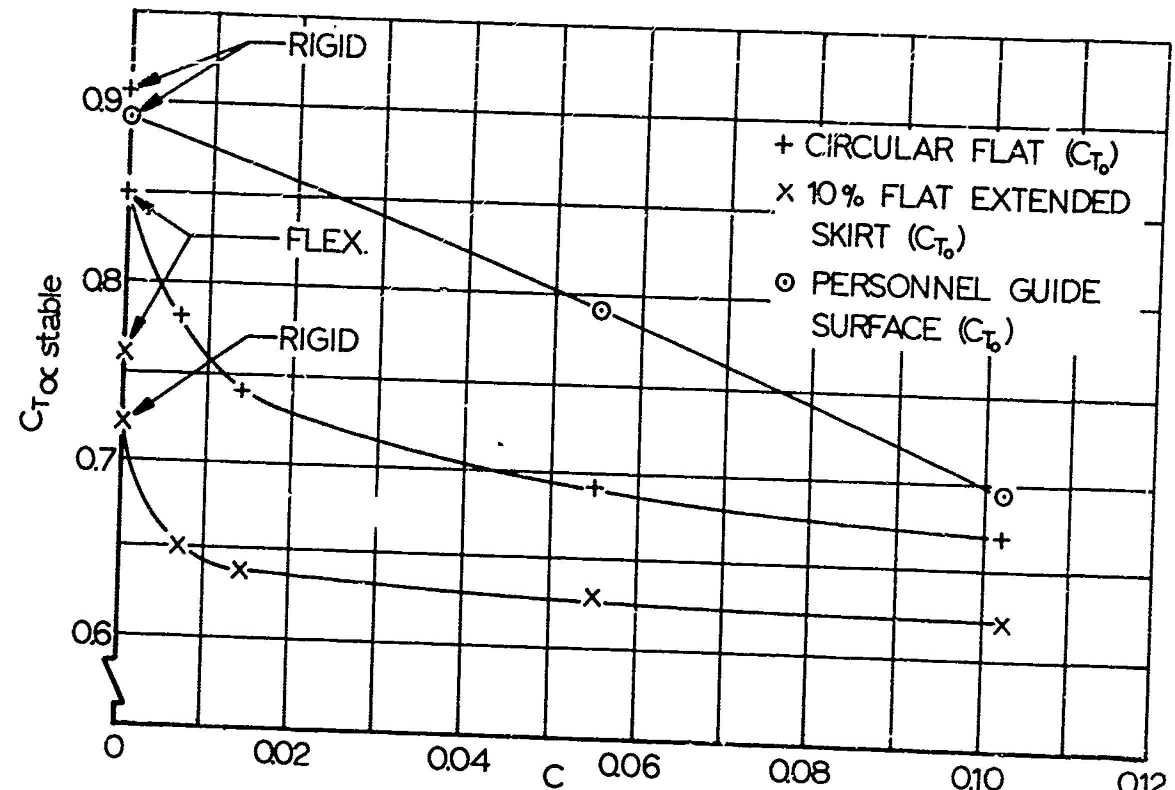

FIG 14. FLAT DESIGN CANOPIES

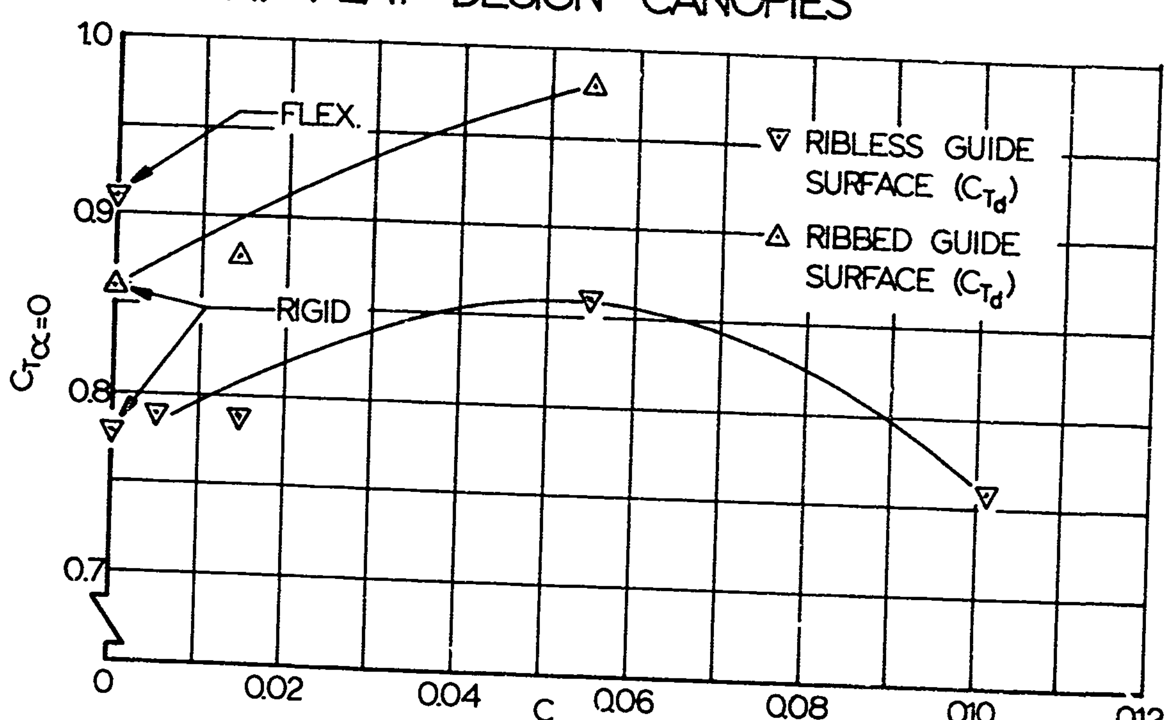

FIG 15. FORMED GORE CANOPIES

TANGENT FORCE COEFFICIENT AT STABLE ANGLE OF ATTACK AS A FUNCTION OF EFFECTIVE POROSITY FOR SEVERAL PARACHUTES to a certain collapse of the guide surfaces. A guide surface parachute with collapsed guide surfaces differs in shape considerably from a fully inflated one as Fig 16 indicates.

It may be noted that the rigid and polyethylene guide surface parachutes deviate from the pattern set by the preceding cloth parachutes. However, since the polyethylene canopy is not stable about zero angle of attack (Fig A-6, Appendix A), and since the rigid models differ considerably from the inflated shapes of the fabric models, these two data points are somewhat insignificant. The results indicate, however, that a ribless guide surface parachute also needs a certain porosity in order to be statically stable.

The preceding analysis was primarily concerned with the stable angle of attack and the related drag coefficient. As mentioned earlier, the slope of the moment curve is another important characteristic. For example, an inspection of the graphs in Appendix A indicates that the circular flat parachute, generally known to be unstable at zero angle of attack, has no side force ($C_N = 0$) and no deflecting moment ($C_M = 0$) at zero angle of attack. However, the slope $dC_M/d\alpha$ is positive, and therefore this parachute will not descend with zero angle of attack without violent oscillations. The moment derivative is also a significant factor in the calculation of dynamic stability. Therefore, the values of $dC_M/d\alpha$ at zero angle of attack of the cloth parachutes under discussion are shown in Fig 17 as a function of effective porosity. Here a high negative value indicates a strong stability at zero angle of attack, while a positive derivative indicates instability. The same results are numerically presented in Table 3.

In a similar manner, Fig 18 shows the change of the drag coefficient, $C_{T_{\alpha=0}} = C_D$, with effective porosity.

For performance analysis, one could go one step further and establish the derivatives $\frac{(dC_M/d\alpha)_{\alpha=0}}{dC}$ and

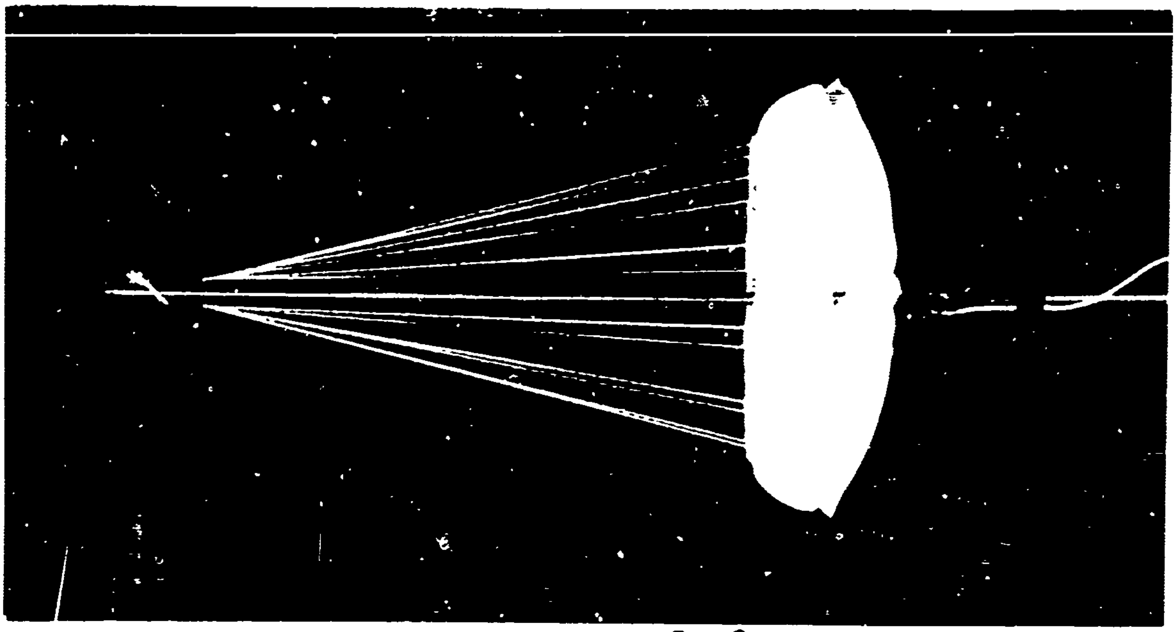

A. NOMINAL POROSITY = 30 FT^3/FT^2-MIN

NOT REPRODUCIBLE

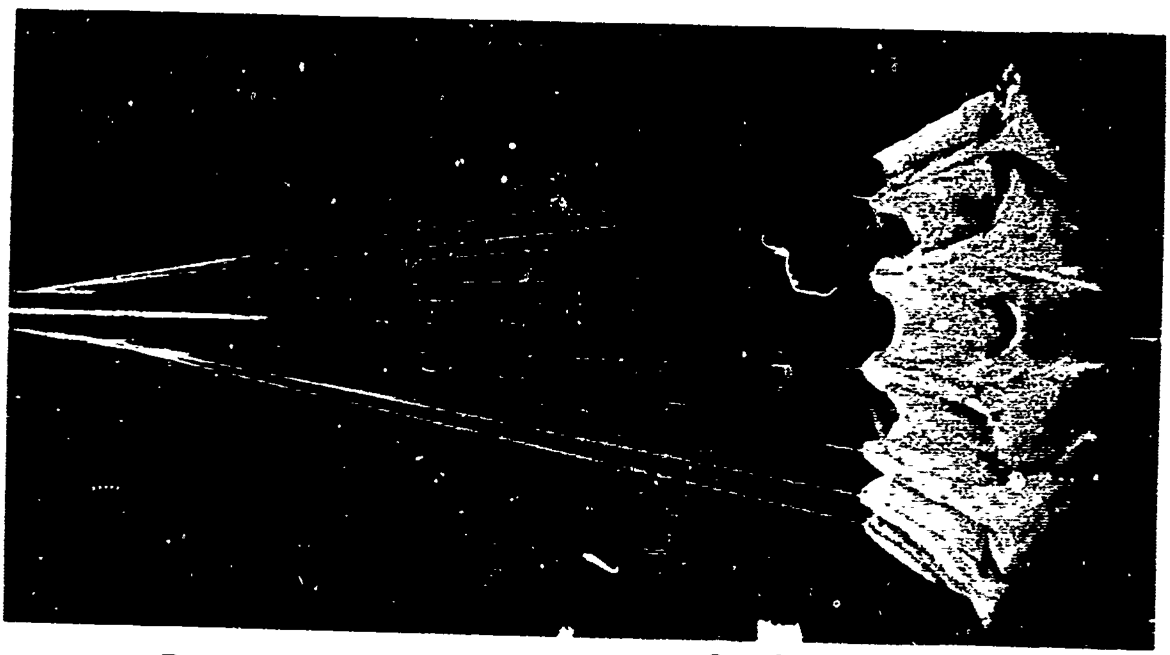

B. NOMINAL POROSITY = 275 FT^3/FT^2-MIN

FIG 16. MODELS OF A RIBLESS GUIDE SURFACE PARACHUTE IN WIND TUNNEL

REYNOLD'S NO. ≅ 6×10^5

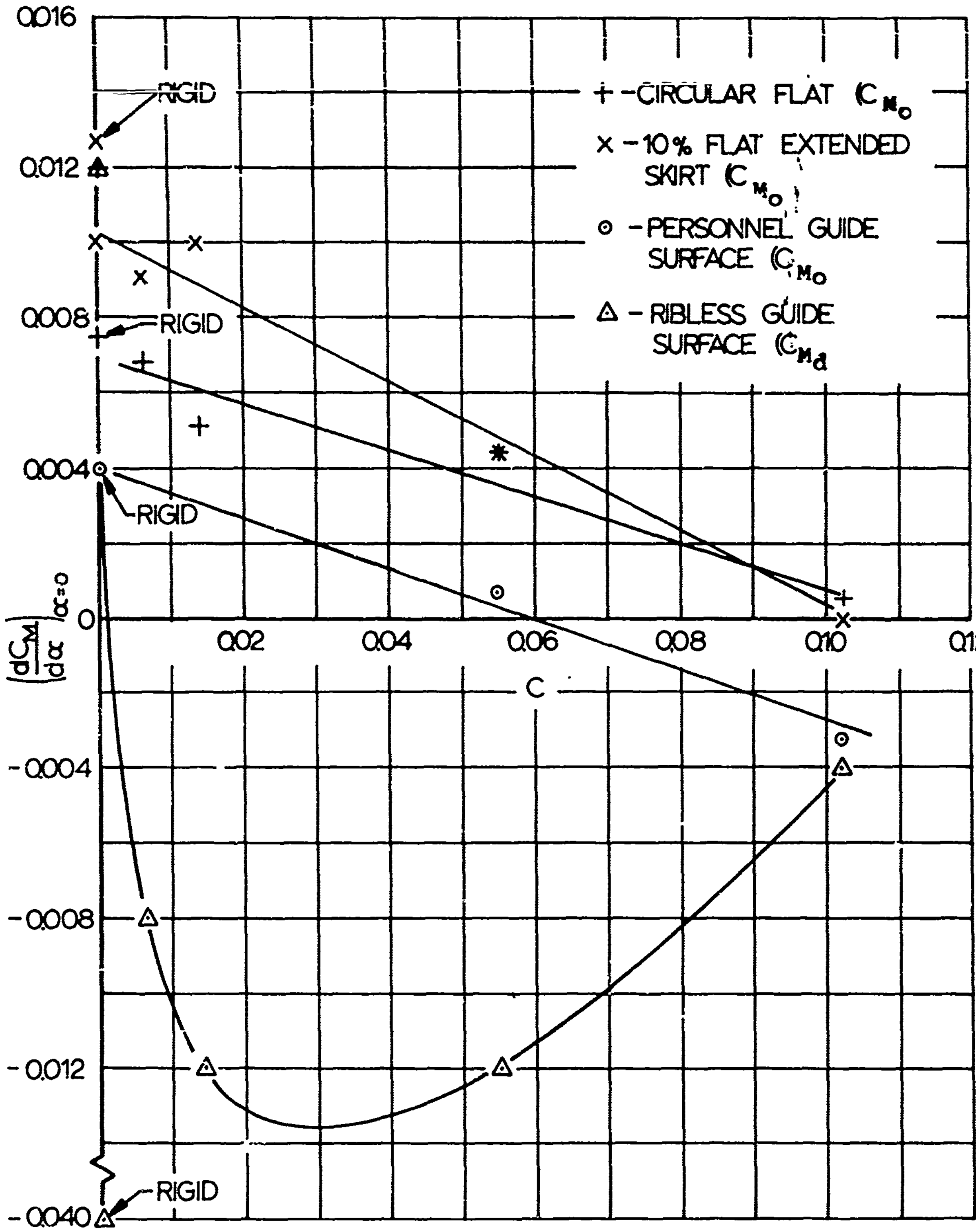

FIG 17. SLOPE OF MOMENT COEFFICIENT CURVE AT ZERO ANGLE OF ATTACK VERSUS EFFECTIVE POROSITY FOR SEVERAL PARACHUTES

Parachute Type	Effective* Porosity	Nominal** Porosity	$(dC_M/d\alpha)_{\alpha=0}$ deg^{-1}	$C_{D\alpha=0}$
Circular Flat (C_{M_o}, C_{D_o})	0.1020	275	+.0004	0.6[illegible]0
	0.0550	120	+.0044	0.690
	0.0140	30	+.0052	0.670
	0.0062	10	+.0068	0.730
	0	0 (Rigid)	+.0076	0.680
	0	0	+.0120	0.780
10% Extended Skirt (C_{M_o}, C_{D_o})	0.1020	275	0	0.614
	0.0550	120	+.0044	0.626
	0.0140	30	+.0100	0.614
	0.0062	10	+.0092	0.594
	0	0(Rigid)	+.0128	0.585
	0	0	+.0100	0.684
Personnel Guide Surface (C_{M_o}, C_{D_o})	0.1020	275	-.0032	0.700
	0.0550	120	+.0008	0.787
	0	0 (Rigid)	+.0040	0.837
Ribless Guide Surface (C_{M_d}, C_{D_d})	0.1020	275	-.0040	0.754
	0.0550	120	-.0120	0.861
	0.0140	30	-.0120	0.788
	0.0062	10	-.0080	0.784
	0	0 (Rigid)	-.0400	0.779
	0	0	+.0120	0.908

* at $\Delta P = 3''\ H_2O$ (test condition) ** at $\Delta P = \frac{1}{2}''\ H_2O$

TABLE 3. STABILITY AND DRAG PARAMETERS AT ZERO ANGLE OF ATTACK

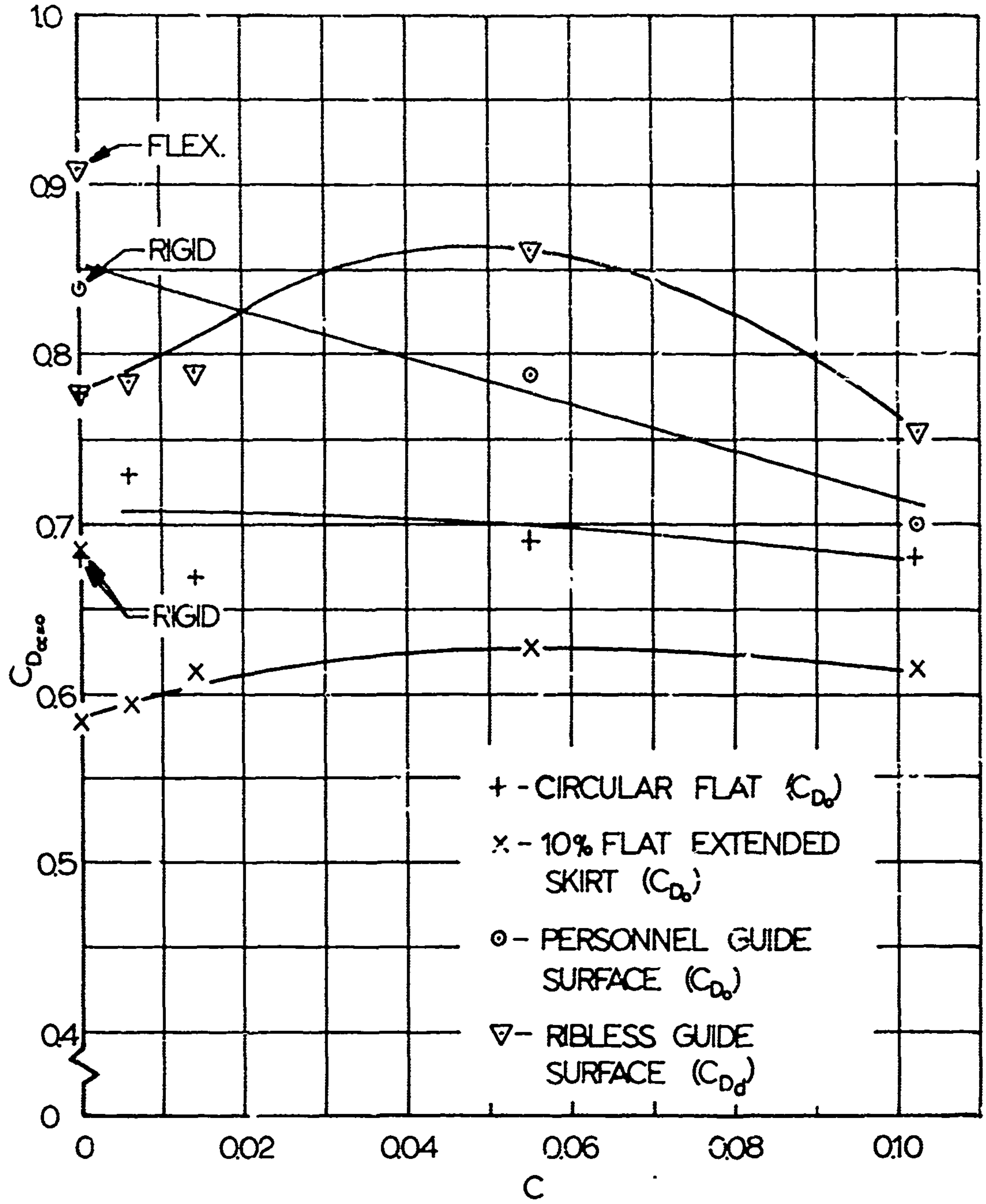

FIG 18. DRAG COEFFICIENT AT ZERO ANGLE OF ATTACK AS A FUNCTION OF EFFECTIVE POROSITY FOR SEVERAL PARACHUTES

$\frac{(dC_D)_{\alpha} = 0}{dC}$ and one would have the changes of the aerodynamic parameters with effective porosity. The detailed investigation of the effective porosity (Ref 1) showed the relationship

$$C = C_o \sigma^n$$

in which C_o is the effective porosity under sea level density, σ, the density ratio, and n an experimental factor. Combining then this relationship, or values extracted from Fig 8, with the pertinent data presented in this report, one can predict the performance characteristics of solid cloth parachutes under various environmental and functional conditions.

LIST OF REFERENCES

1. Heinrich, H. G.: Some Research Efforts Related to Problems of Aerodynamic Deceleration, WADD TN 60-276, November, 1960.

2. Performance of and Design Criteria for Deployable Aerodynamic Decelerators, ASD-TR-61-579, December 1963, AD 429 971.

3. Heinrich, H. G.: Investigation of Stability of Parachutes and Development of Stable Parachutes from Fabrics of Normal Porosity, Report No. 300, March 23, 1943, with German text (GZF Guide Surface Parachute) ASTIA ATI 42978.

4. Topping, A. D., Marketos, J. D., and Costakos, N. C.: A Study of Canopy Shapes and Stresses for Parachutes in Steady Descent, WADC TR 55-294, October, 1955.

5. Drag and Stability of Parachutes, Aeronautical Engineering Review, June, 1956, pp 73-79.

6. Ross, R. S. and Stimler, F. J.: Drop Tests of 16,000 Sq. In. Model Parachutes, Volume VIII, ASTIA AD 45583.

7. Heinrich, H. G.: Memorandum Report on Parachutes, Guide Surface, 10 February 1948, ATI 28935.

8. Heinrich, H. G.: Aerodynamics, Performance, and Design of Personnel Guide Surface Parachute, November 21, 1951,(Report No. WCEE 672-145-A-9-1).

APPENDIX A

TANGENT FORCE, NORMAL FORCE, AND MOMENT COEFFICIENTS OF CONVENTIONAL PARACHUTE TYPES

This section contains the complete data from wind tunnel tests on ten conventional type parachutes fabricated from different materials. For the most part, these tests were made at a Reynolds number of 6×10^5 and a Mach number of 0.1. The exceptions are noted individually.

Included in this section is Table A-1 which gives the complete nomenclature of all models used in the study and a number of constants used in data reduction.

Although Table A-1 shows that both a metal and a cloth model of the ribbon parachute with 30% geometric porosity and 50" prototype diameter were tested, results are presented for only the rigid metal model. The cloth model did not inflate at any angle of attack, as seen in Fig A-12.

The nominal porosity "b" (ft^3/ft^2-min) obtained under a differential pressure of 1/2 inch of water can be converted to the effective porosity for the same differential pressure by the equation

$$C = (3.57 \times 10^{-4})b \quad . \qquad (A.1)$$

PARACHUTE TYPE	Canopy Material Specification	Geometric Porosity %	Nominal Porosity ft³/ft²-min	Nominal Diameter D_o in	Canopy Surf. Area S_o in²	Design Diameter D_d in	Number of Gores	Suspension Line Length L in	① Projected Diameter D_p in	② Projected Canopy Area S_p in²	Canopy Depth h in	Total Model Lgth. d in	Angle of Canopy Collapse Deg	Dynamic Pressure q lb/ft²	Moment Arm ③ K_o in	Moment Arm ④ K_p in	Moment Arm ⑤ K_d in
Circular Flat	0.064 in. thick 1430 Aluminum sheet		0	16.6	218			12	12.0	113	4.88	16.0		12.6	1.79		
10% Extended Skirt				17.3	233			12			5.19	16.0			1.87		
14.3% Extended Skirt				19.3	294			10			7.25	16.3			2.23		
Conical				17.3	235			11			6.63	16.2			2.00		
Personnel Guide Surface	0.064 in. annealed Copper sheet			15.7	193			12			4.94	15.6			1.72		
Ribless Guide Surface	0.051 in. cold roll. Steel sheet					12.5		12			4.19	17.1				1.68	1.75
Ribless Guide Surface with Spoilers						12.6		12			4.19	16.6				1.68	1.75
Ribbed Guide Surface	0.051 in. annealed Copper sheet					17.0		12			4.13	16.6				1.67	1.67
Ribbon 20% Porosity 50 in. Prototype	0.064 in. thick 1430 Aluminum sheet	19.3		16.6	219			12			4.88	16.0			1.79		
Ribbon 20% Porosity 100 in. Prototype		19.4						12									
Ribbon 30% Porosity 50 in. Prototype		28.6						12									
Ringslot 20% Porosity 50 in. Prototype		20.9						12									
Ringslot 20% Porosity 100 in. Prototype		19.8						12									
Ringslot 30% Porosity 50 in. Prototype		28.8						12									
Circular Flat	1.1 oz/yd, 40#/in. Tensile Str. Nylon		120	16.3	209		28	17.3	12.3	118	4.60	21.9	38		.74		
Circular Flat			10	16.3	209			17.3	12.1	115	4.80	22.1	47		1.76		
Circular Flat	Rayon		275	16.2	206			16.5	11.9	111	4.40	22.1	22		1.72		
Circular Flat	0.0015 in. thick Polyethylene		0	16.1	205			16.1	12.0	114	5.35	21.3	50		1.79		
Circular Flat			30	16.3	207			16.5			4.75	21.0	45	4.18	1.75		
10% Extended Skirt	1.1 oz/yd, 40#/in. Tensile Str. Nylon		120	18.7	275			17.1	13.2	136	5.50	22.8	37	12.6	2.02		
10% Extended Skirt			10	19.7	306			16.5	13.3	138	5.85	21.9	49		2.08		
10% Extended Skirt	Rayon		275	19.2	290			17.0	13.9	152	5.50	22.4	[illegible]		2.06		
10% Extended Skirt			30	19.3	291						5.30	22.0	44	4.18	2.05		
10% Extended Skirt	0.0015 in. thick Polyethylene		0	18.8	279			14.5	13.1	135	4.4	19.4	50	4.18	1.94		

TABLE A-1. FORMED METAL AND FABRIC PARACHUTE SPECIFICATIONS

PARACHUTE TYPE	Canopy Material Specifications	Geometric Porosity λ	Nominal Porosity r ft³/ft²-min	Nominal Diameter D_o in	Canopy Surf. Area S_o in²	Design Diameter D_d in	Number of Gores	Suspension Line Length L in	Projected Diameter ① D_p in	Projected ② Canopy Area S_p in²	Canopy Depth h in	Total Model Lgth. d in	Angle of Canopy Collapse Deg	Dynamic Pressure q lb/ft²	Moment Arm ③ K_o in	Moment Arm ④ K_p in	Moment Arm ⑤ K_d in
14.3% Extended Skirt	1.2 oz/yd, 40#/in. Tensile Str. Nylon		120	19.8	306		28	16.9	14.2	159	5.00	23.0	35	12.6	2.06		
14.3% Extended Skirt			10	19.6	302		28	17.0	13.6	144	5.25	23.0	49	4.18	2.07		
Conical	1.1 oz/yd, 40#/in. Tensile Str. Nylon		120	15.0	178		24	17.3	11.1	98	4.80	22.3	37	12.6	1.65		
Conical			30	15.0	178		↓	14.4	10.9	93	4.60	19.1	44	↓	1.63		
Personnel Guide Surface	1.1 oz/yd, 40#/in. Tensile Str. Nylon		120	14.7	170		↓	16.1	11.5	105	4.20	20.5	32	↓	1.57		
Personnel Guide Surface	Rayon		275	14.9	175		↓	16.3	11.3	101	4.80	21.5	20	↓	1.64		
Ribless Guide Surface	1.1 oz/yd, 40#/in. Tensile Str. Nylon		120			12.6	12	16.1	11.8	110	4.00	20.5	28	↓		1.65	1.73
Ribless Guide Surface			10			↓	↓	16.5	12.9	130	4.00	20.6	49	↓		1.76	1.73
Ribless Guide Surface	Rayon		275			↓	↓	17.0	10.6	89	4.00	21.7	11	↓		1.51	1.73
Ribless Guide Surface			30			↓	↓	16.3	11.8	110	4.00	23.5	40	↓		1.65	1.73
Ribless Guide Surface	0.0015 in. thick Polyethylene		0			↓	↓	16.9	13.0	132	4.00	20.8	23	↓		1.77	1.73
Ribbed Guide Surface	1.1 oz/yd, 40#/in. Tensile Str. Nylon		120			12.0	↓	16.9	13.0	132	5.00	22.1	25	↓		1.85	1.75
Ribbed Guide Surface			30			12.0	↓	16.5	12.9	131	5.00	21.8	40	↓		1.85	.75
Ribless Guide Surface with Spoilers	1.1 oz/yd, 40#/in. Tensile Str. Nylon		120			12.6	↓	16.5	11.8	108	4.00	20.8	23	↓		1.64	1.73
Ribless Guide Surface with Spoilers			30			12.6	↓	16.9	12.1	115	4.00	20.5	30	↓		1.68	1.73
Ribbon 20% Porosity 50 in. Prototype	5/8 in. Tape Class 8, Type 3	19.5		15.8	197		20	17.0	11.7	107	4.40	21.9	14	↓	1.69		
Ribbon 20% Porosity 100 in. Prototype	Bally Ribbon Mills	19.5		15.8	197		↓	17.3	11.6	105	↓	21.9	18	↓	1.69		
Ribbon 30% Porosity 50 in. Prototype	Bally Ribbon Mills	29.8					↓				↓		All Angles	↓			
Ringslot 20% Porosity 50 in. Prototype	1-1/4 in. Tape Class C, Type 4	20.1		15.8	197		↓	16.8	12.1	115	↓	21.1	24	↓	1.69		
Ringslot 20% Porosity 100 in. Prototype		20.2		16.0	201		↓	16.6	12.1	115	↓	21.3	21	↓	1.70		
Ringslot 30% Porosity 50 in. Prototype		28.6		15.7	194		↓	15.1	12.1	115	↓	29.7	18	↓	1.68		

Note: ① Max. distance between centers of opposing gores ② $S_p = \pi D_p^2/4$ ③ $K_o = h + D_o$ ④ $K_p = h + 1.33\,D_p$ ⑤ $K_d = h + 1.33\,D_d$

TABLE A-1 CONTINUED

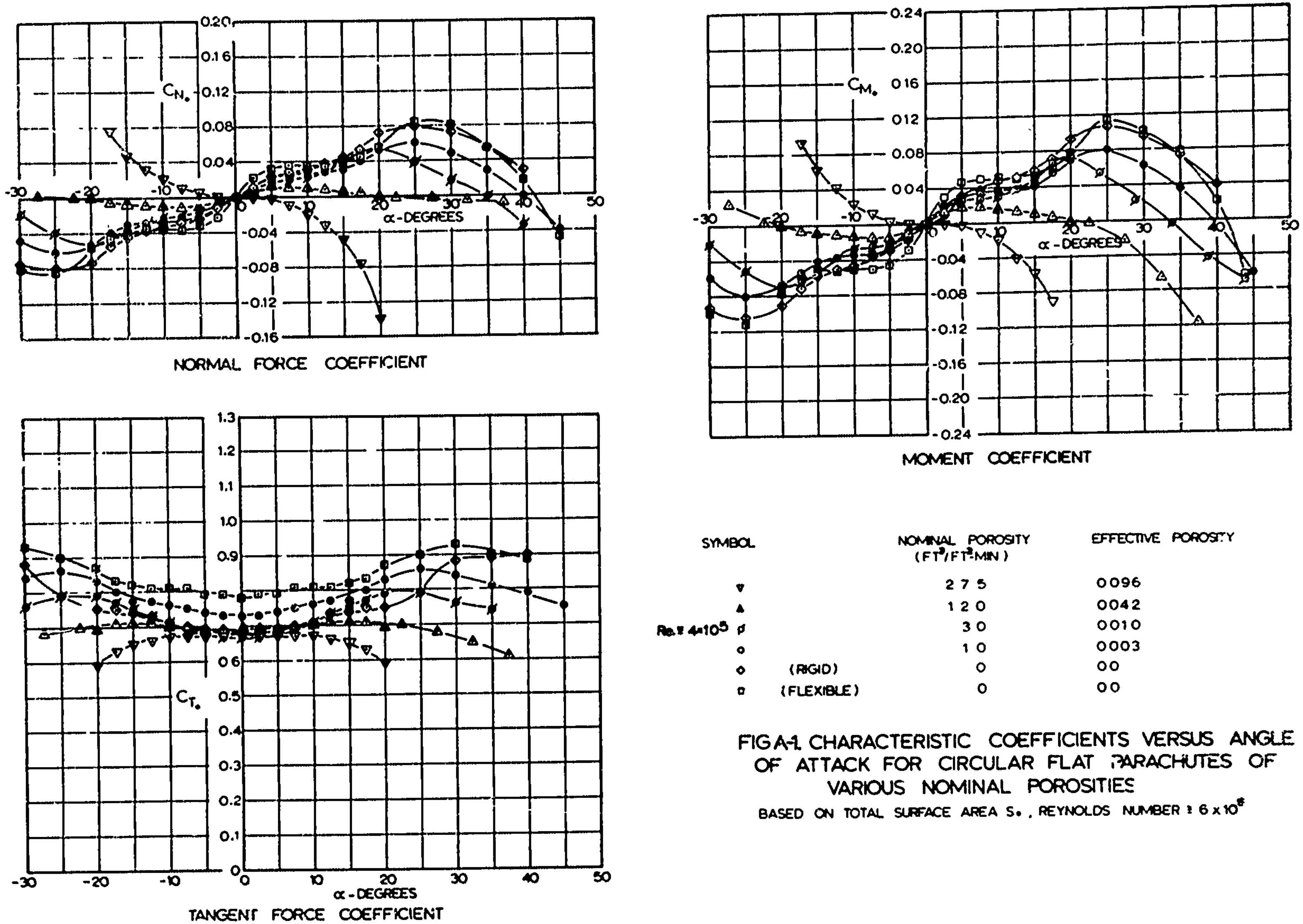

SYMBOL		NOMINAL POROSITY (FT³/FT²-MIN)	EFFECTIVE POROSITY
▼		2 7 5	0096
▲		1 2 0	0042
Re ≅ 4×10⁵ ø		3 0	0010
○		1 0	0003
◇	(RIGID)	0	00
□	(FLEXIBLE)	0	00

FIG A-1. CHARACTERISTIC COEFFICIENTS VERSUS ANGLE OF ATTACK FOR CIRCULAR FLAT PARACHUTES OF VARIOUS NOMINAL POROSITIES

BASED ON TOTAL SURFACE AREA S_o, REYNOLDS NUMBER ≅ 6×10^5

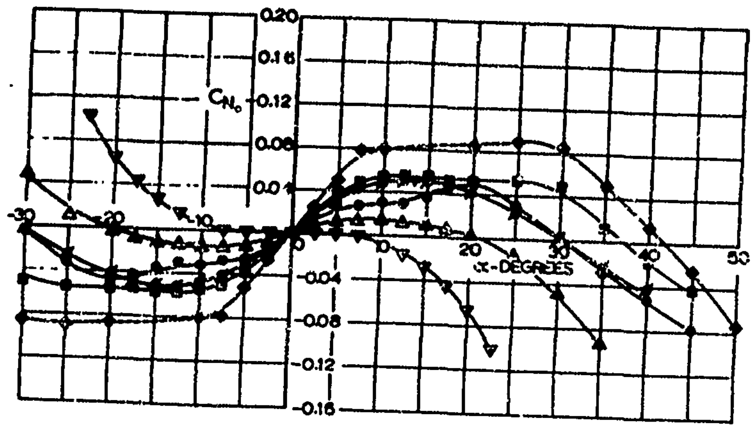

NORMAL FORCE COEFFICIENT

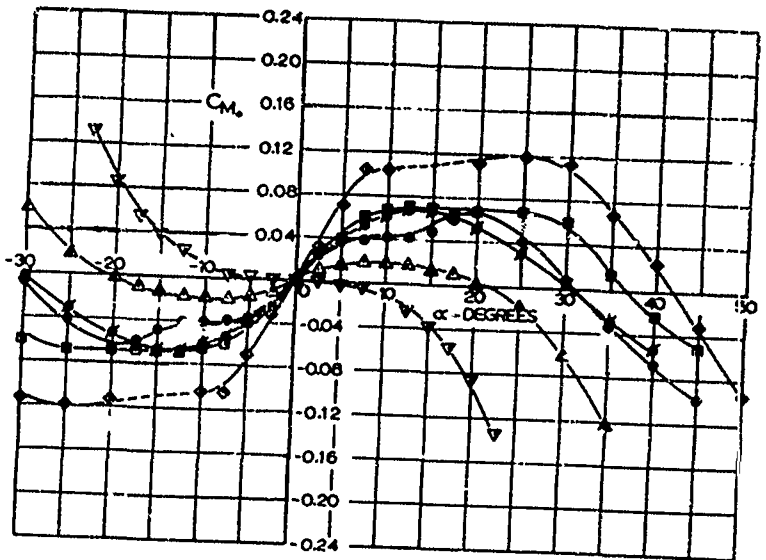

MOMENT COEFFICIENT

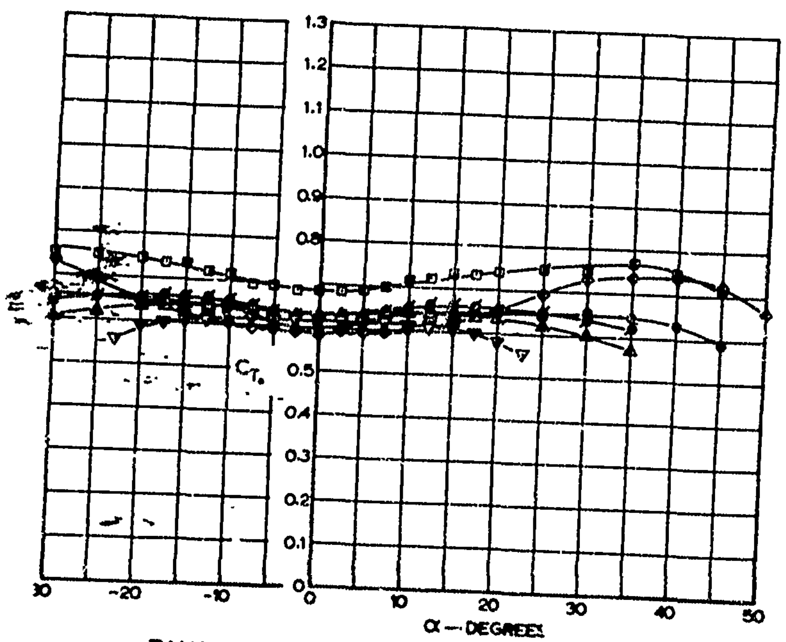

TANGENT FORCE COEFFICIENT

SYMBOL	NOMINAL POROSITY (FT³/FT² MIN)	EFFECTIVE POROSITY
▽	275	0.096
△	120	0.042
Re ≅ 4x10⁵ ⌀	30	0.010
○	10	0.003
◇ (RIGID)	0	0.0
Re. ≅ 4x10⁵ □ (FLEXIBLE)	0	0.0

FIG A-2. CHARACTERISTIC COEFFICIENTS VERSUS ANGLE OF ATTACK FOR 10% FLAT EXTENDED SKIRT PARACHUTES OF VARIOUS NOMINAL POROSITIES

BASED ON TOTAL SURFACE AREA S_o, REYNOLDS NUMBER ≅ 6×10^5

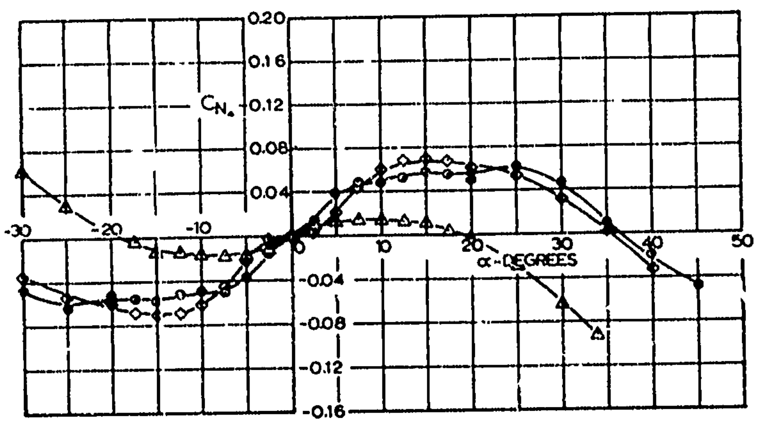

NORMAL FORCE COEFFICIENT

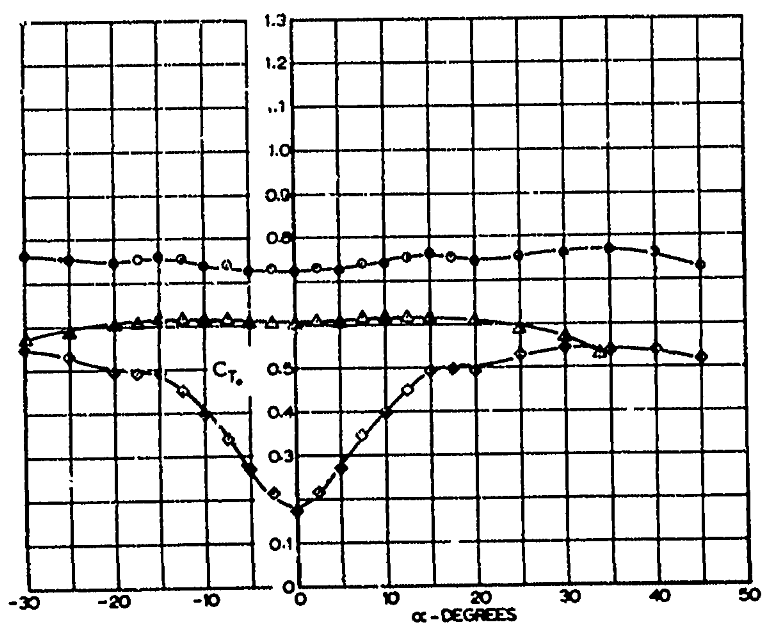

TANGENT FORCE COEFFICIENT

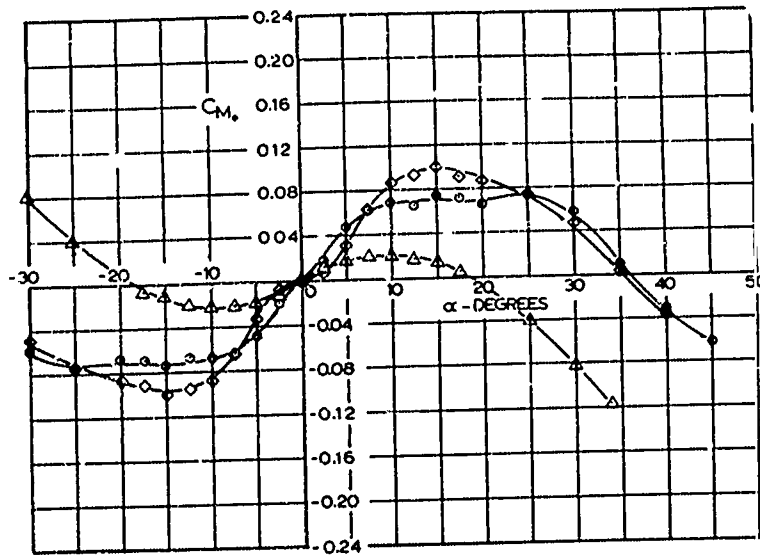

MOMENT COEFFICIENT

SYMBOL	NOMINAL POROSITY (FT^3/FT^2- MIN)	EFFECTIVE POROSITY
Δ	120	0042
$Re = 4x10^5$ ○	10	0.003
◇ (RIGID)	0	00

FIG A-3. CHARACTERISTIC COEFFICIENTS vs. ANGLE OF ATTACK FOR 143% FULL EXTENDED SKIRT PARACHUTES OF VARIOUS NOMINAL POROSITIES.

BASED ON TOTAL SURFACE AREA S_o

REYNOLDS NUMBER = 6×10^5

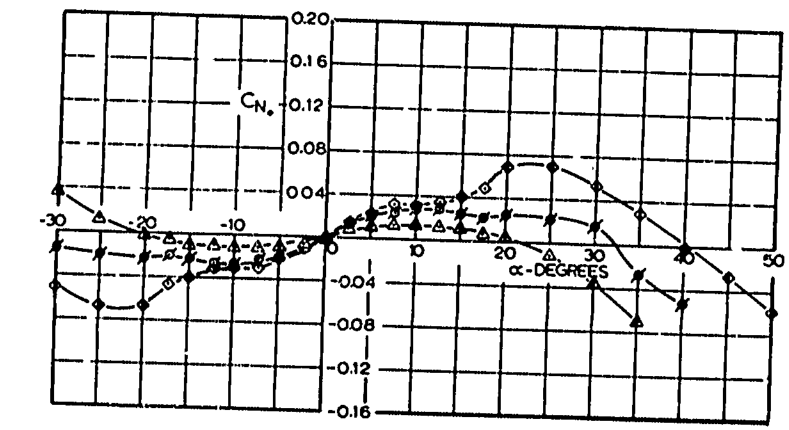

NORMAL FORCE COEFFICIENT

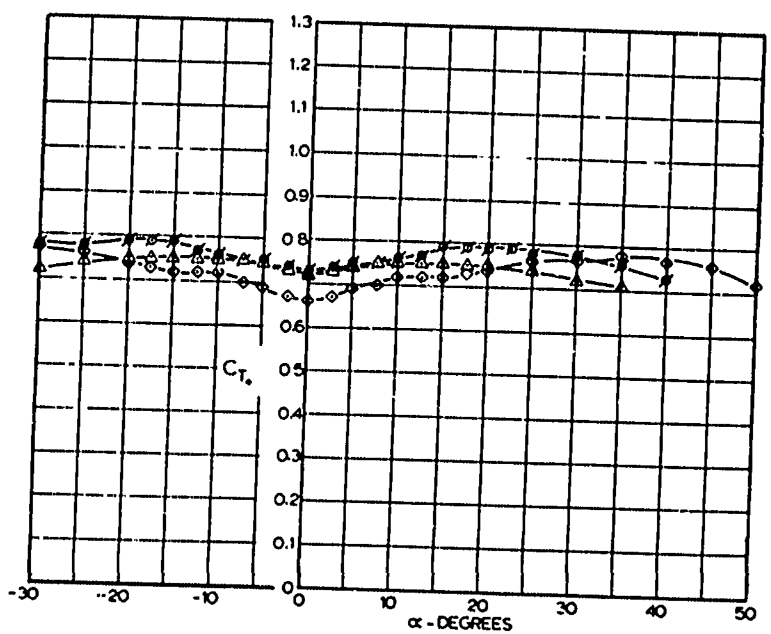

TANGENT FORCE COEFFICIENT

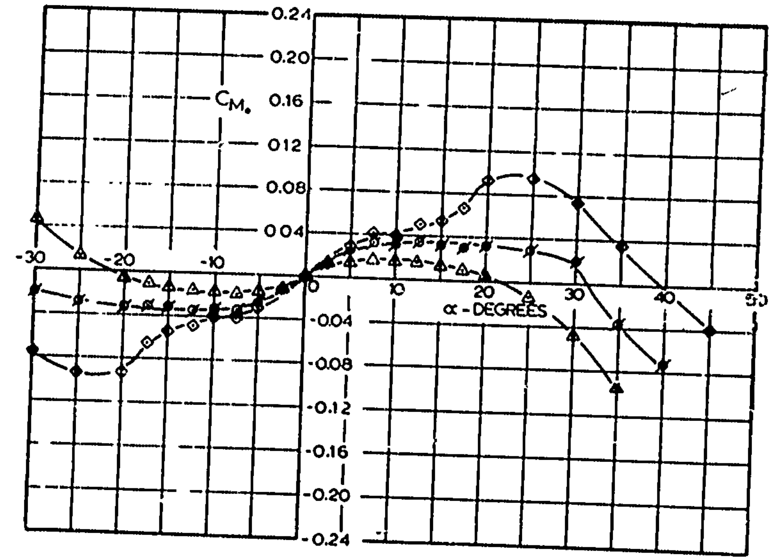

MOMENT COEFFICIENT

SYMBOL		NOMINAL POROSITY (FT^3/FT^2-MIN)	EFFECTIVE POROSITY
△		1 2 0	0 0 4 2
ø		3 0	0 0 1 0
◇	(RIGID)	0	0 0

FIG A-4. CHARACTERISTIC COEFFICIENTS VERSUS ANGLE OF ATTACK FOR CONICAL PARACHUTES OF VARIOUS NOMINAL POROSITIES

BASED ON TOTAL SURFACE AREA S_0, REYNOLDS NUMBER ≈ 6×10^5

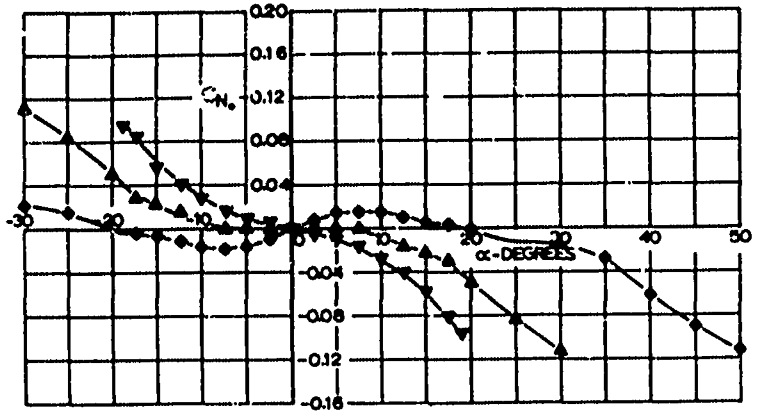

NORMAL FORCE COEFFICIENT

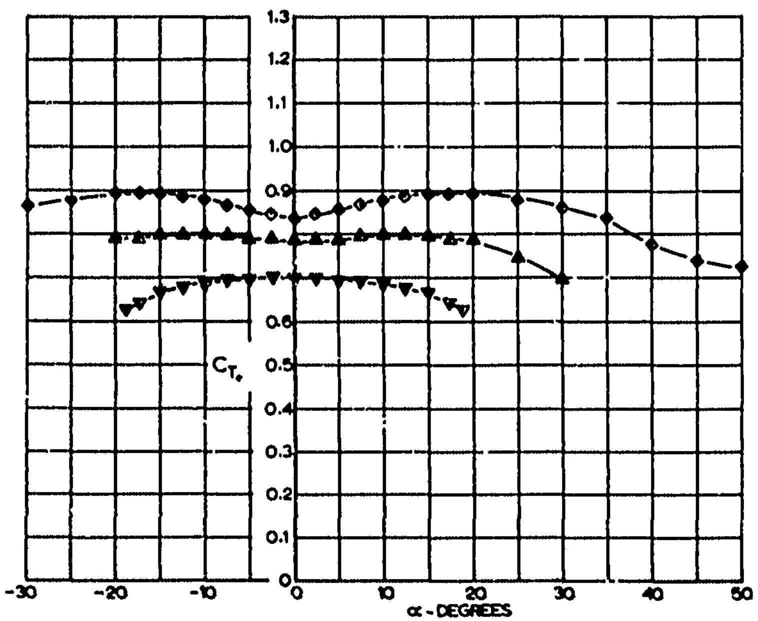

TANGENT FORCE COEFFICIENT

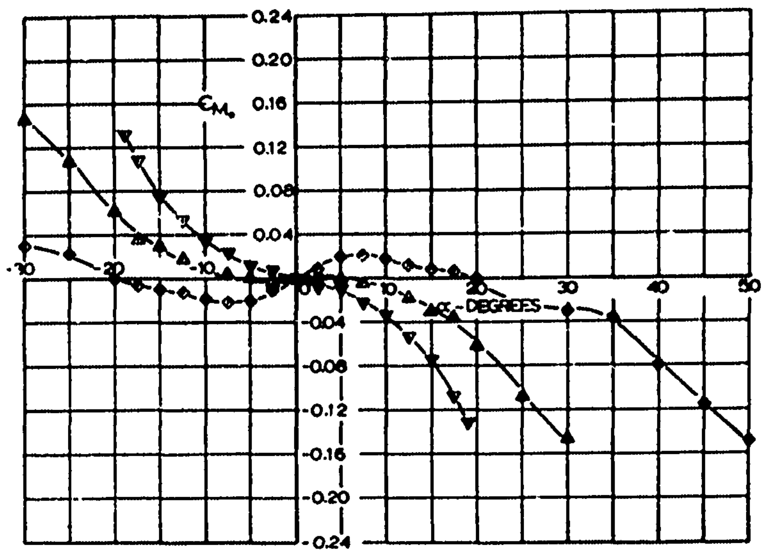

MOMENT COEFFICIENT

SYMBOL	NOMINAL POROSITY (FT^3/FT^2 - MIN)	EFFECTIVE POROSITY
▽	275	0.096
△	120	0.042
◇ (RIGID)	0	0

FIG A-5. CHARACTERISTIC COEFFICIENTS vs. ANGLE OF ATTACK FOR PERSONNEL GUIDE SURFACE PARACHUTES OF VARIOUS NOMINAL POROSITIES.

BASED ON TOTAL SURFACE AREA S_o

REYNOLDS NUMBER: 6×10^5

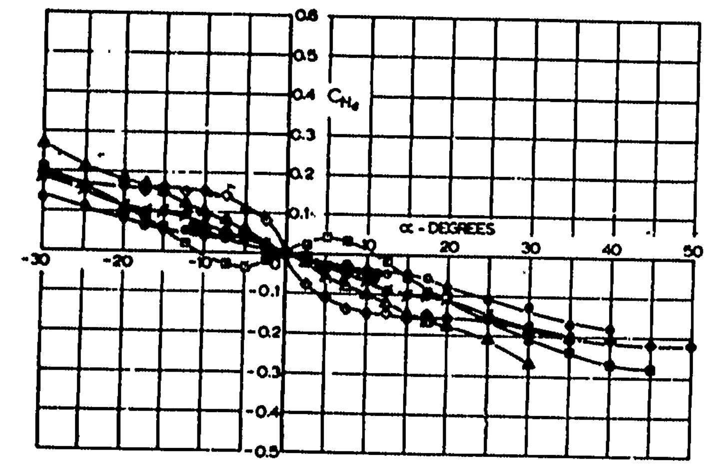

NORMAL FORCE COEFFICIENT

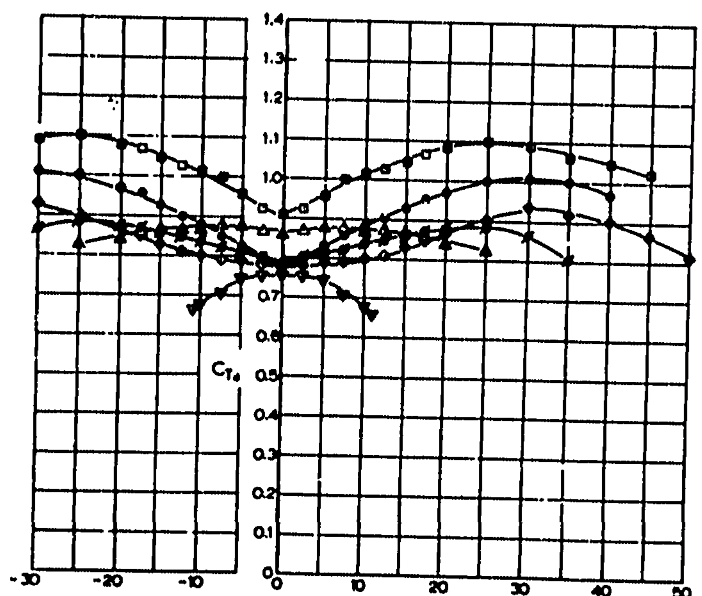

TANGENT FORCE COEFFICIENT

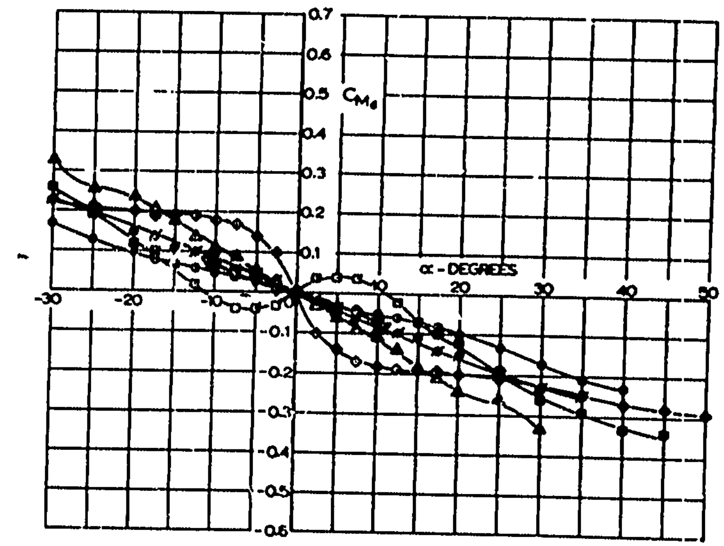

MOMENT COEFFICIENT

SYMBOL	NOMINAL POROSITY (FT³/FT²-MIN)	EFFECTIVE POROSITY
▼	275	0.096
▲	120	0.042
⌀	30	0.010
○	10	0.003
◇ (RIGID)	0	0.0
□ (FLEXIBLE)	0	0.0

FIG A-6 CHARACTERISTIC COEFFICIENTS VERSUS ANGLE OF ATTACK FOR RIBLESS GUIDE SURFACE PARACHUTES OF VARIOUS NOMINAL POROSITIES

BASED ON DESIGN DIAMETER D_d, REYNOLDS NUMBER ≈ 6×10^5

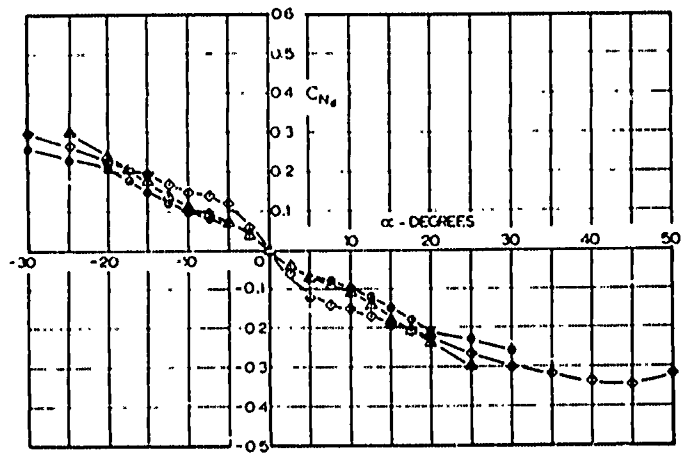

NORMAL FORCE COEFFICIENT

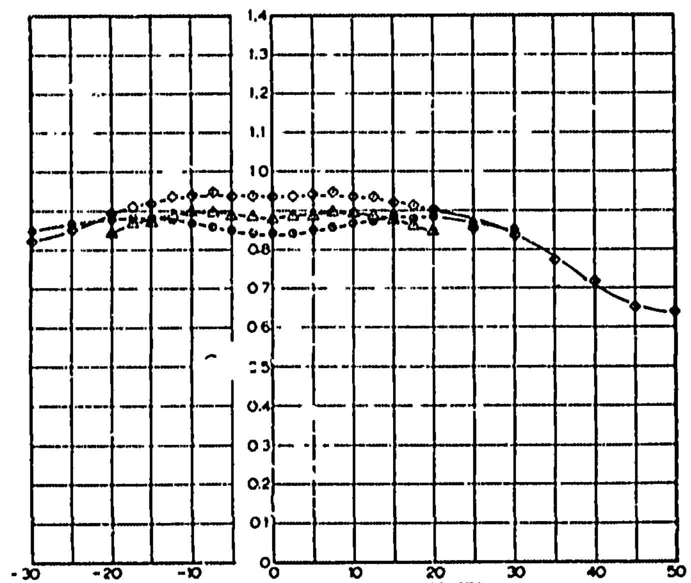

TANGENT FORCE COEFFICIENT

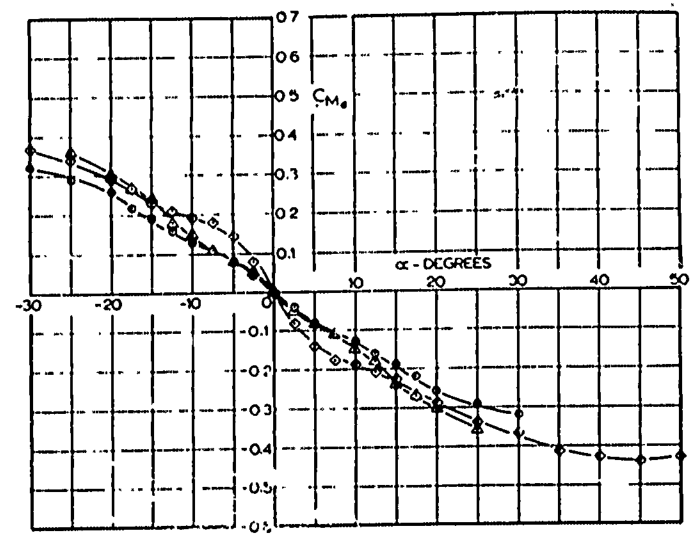

MOMENT COEFFICIENT

SYMBOL	NOMINAL POROSITY (FT^3/FT^2-MIN)	EFFECTIVE POROSITY
▲	120	0.042
○	30	0.010
◇ (RIGID)	0	0.0

FIG A-7. CHARACTERISTIC COEFFICIENTS VERSUS ANGLE OF ATTACK FOR RIBLESS GUIDE SURFACE PARACHUTES WITH SPOILERS FOR VARIOUS NOMINAL POROSITIES

BASED ON DESIGN DIAMETER D_d

REYNOLDS NUMBER ≈ 6×10^5

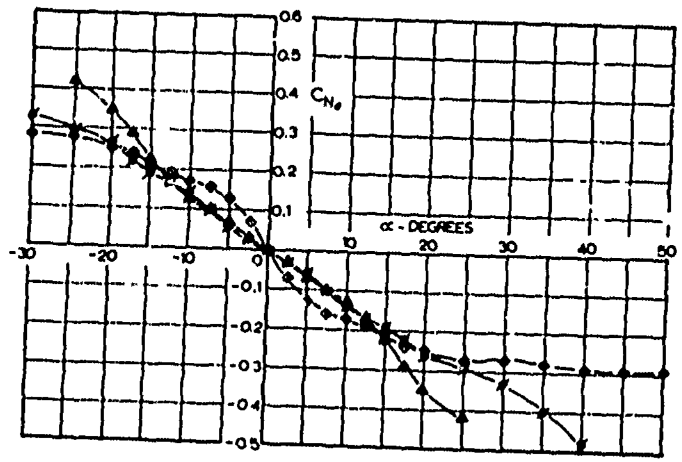

NORMAL FORCE COEFFICIENT

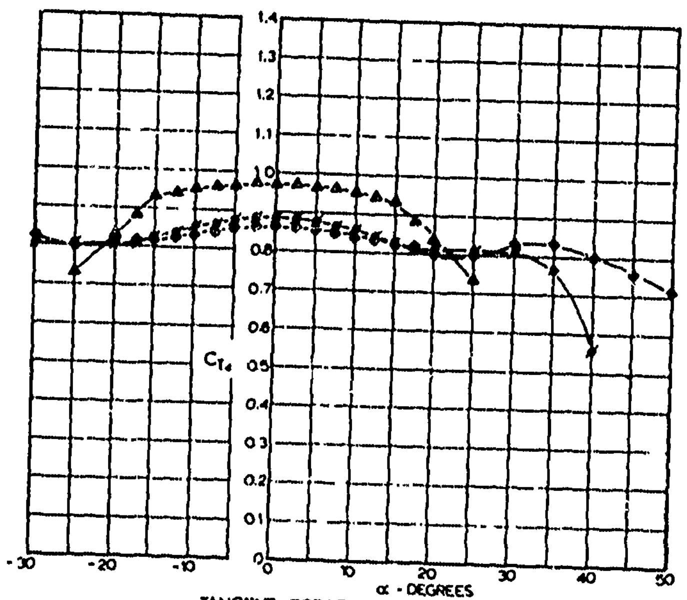

TANGENT FORCE COEFFICIENT

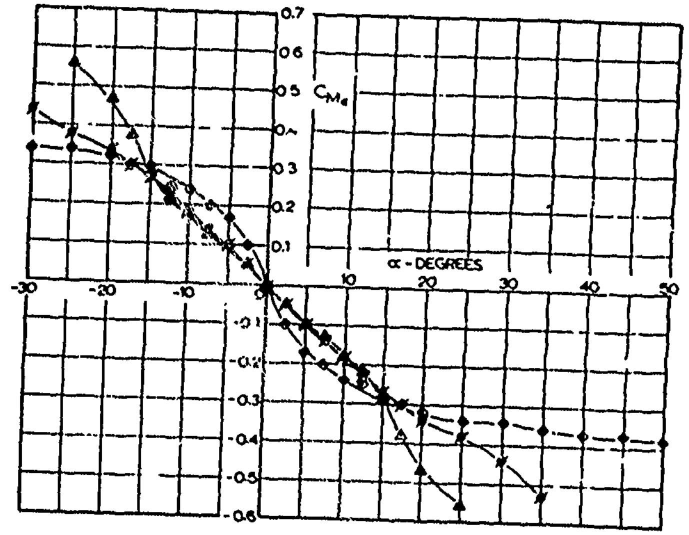

MOMENT COEFFICIENT

SYMBOL	NOMINAL POROSITY (FT^3/FT^2 - MIN)	EFFECTIVE POROSITY
▲	120	0042
ø	30	0010
◆ (RIGID)	0	00

FIG A-8. CHARACTERISTIC COEFFICIENTS vs ANGLE OF ATTACK FOR RIBBED GUIDE SURFACE PARACHUTES OF VARIOUS NOMINAL POROSITIES

BASED ON DESIGN DIAMETER D_d
REYNOLDS NUMBER ≈ 6×10^5

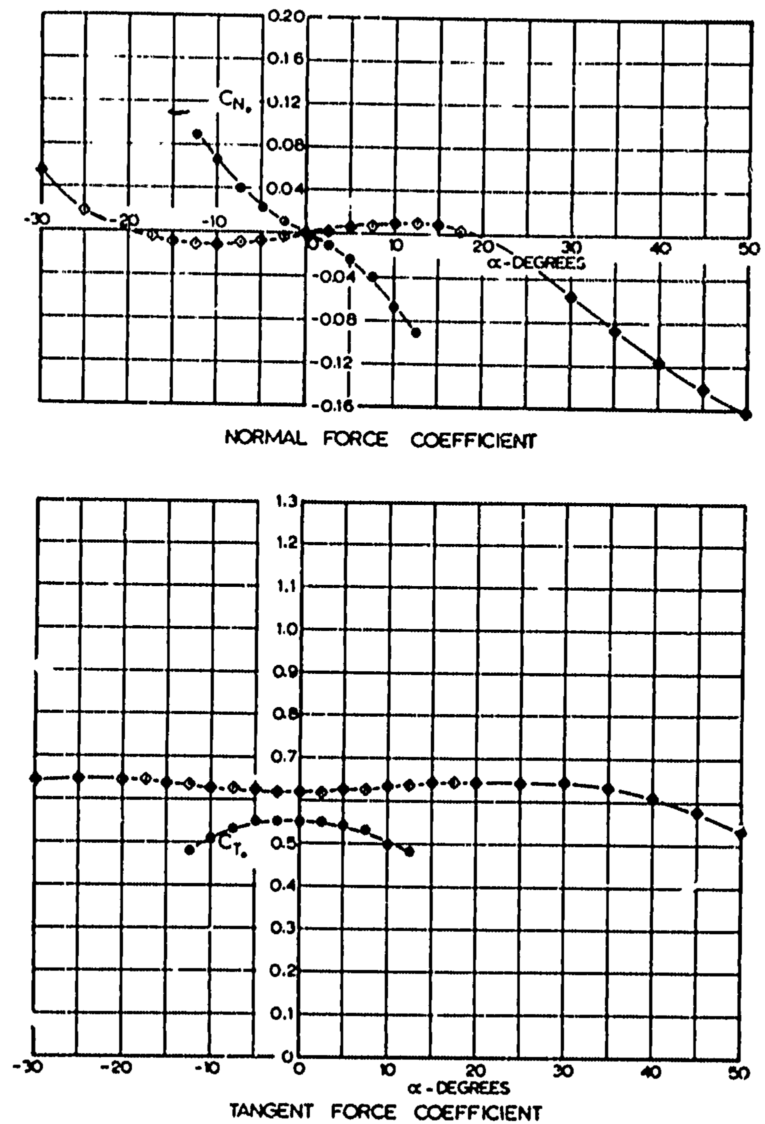

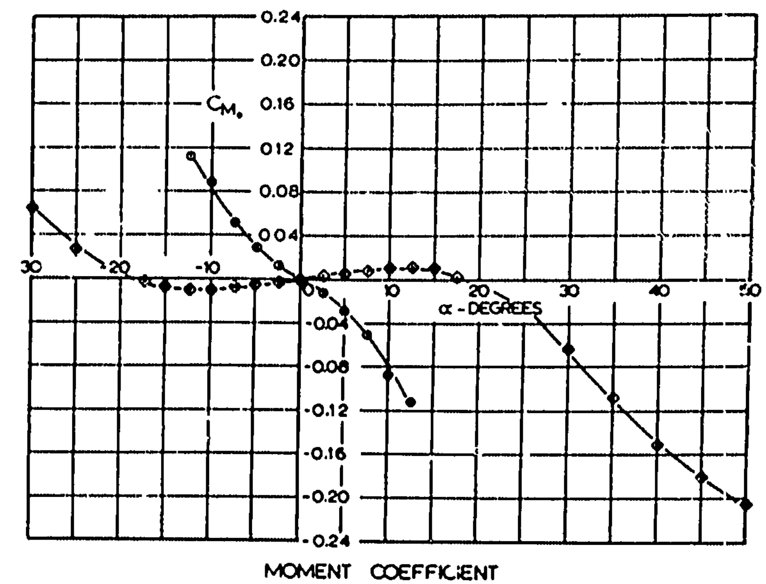

o — FLEXIBLE FABRIC MODEL

◇ — RIGID METAL MODEL

FIG A-9. CHARACTERISTIC COEFFICIENTS vs ANGLE OF ATTACK FOR 50' PROTOTYPE DIAMETER RIBBON PARACHUTE OF 20% GEOMETRIC POROSITY

BASED ON TOTAL SURFACE AREA S_o

REYNOLDS NUMBER = 6×10^5

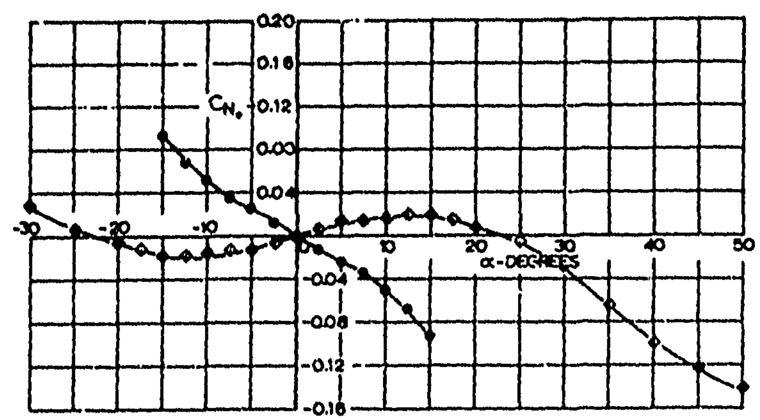

NORMAL FORCE COEFFICIENT

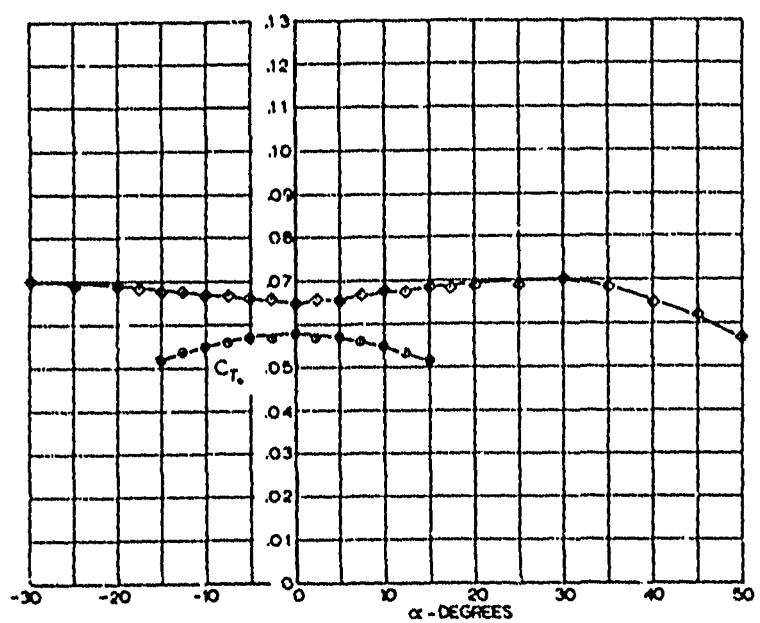

TANGENT FORCE COEFFICIENT

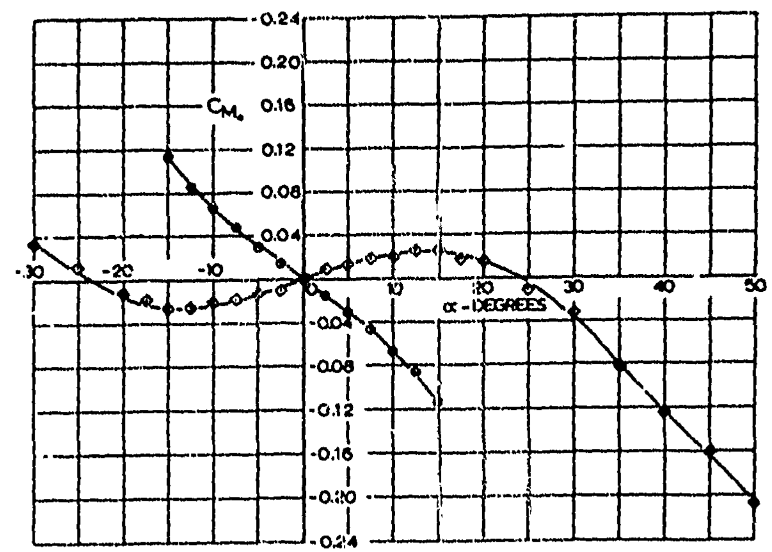

MOMENT COEFFICIENT

◆ - RIGID METAL MODEL

○ - FLEXIBLE FABRIC MODEL

FIG A-10 CHARACTERISTIC COEFFICIENTS vs. ANGLE OF ATTACK FOR 100" PROTOTYPE DIAMETER RIBBON PARACHUTE OF 20 % GEOMETRIC POROSITY

BASED ON TOTAL SURFACE AREA S_o

REYNOLDS NUMBER ≈ 6×10^5

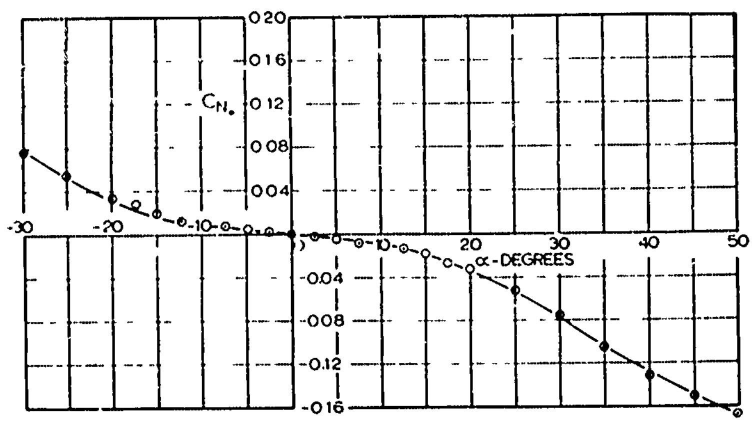

NORMAL FORCE COEFFICIENT

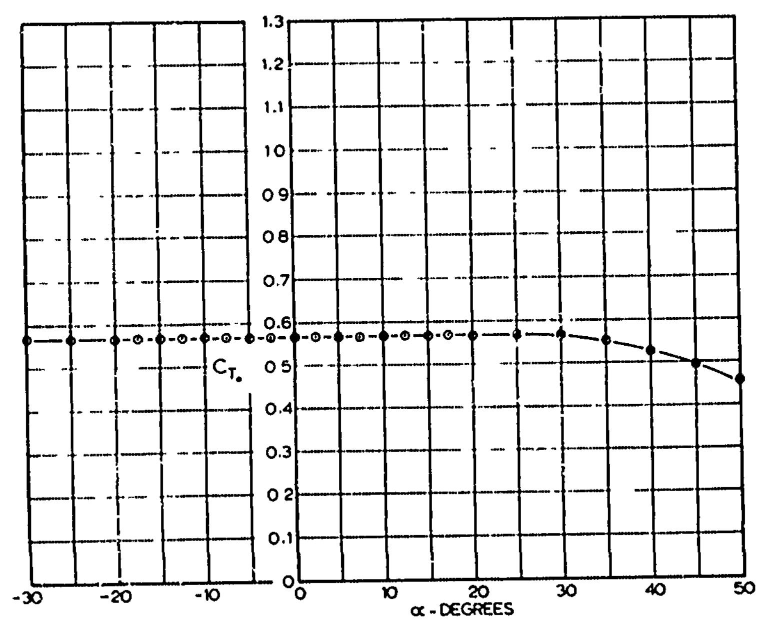

TANGENT FORCE COEFFICIENT

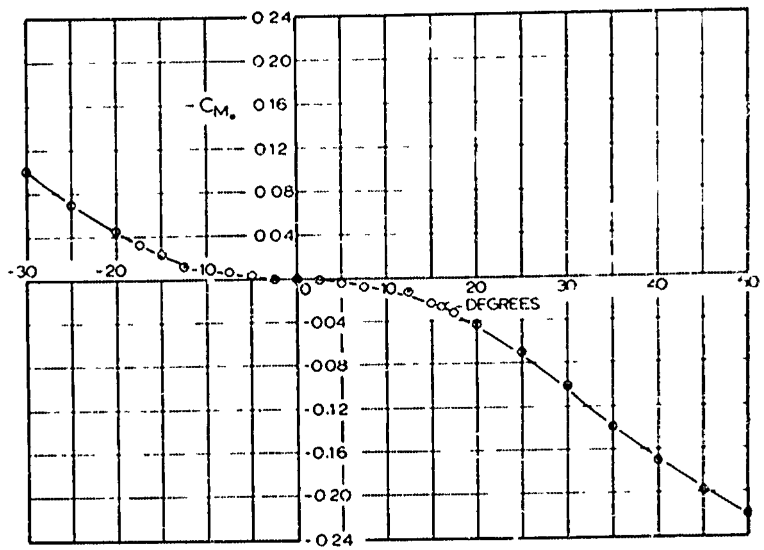

MOMENT COEFFICIENT

o RIGID METAL MODEL

FIG A-11. CHARACTERISTIC COEFFICIENTS vs ANGLE OF ATTACK FOR 50" PROTOTYPE DIAMETER RIBBON PARACHUTE OF 30% GEOMETRIC POROSITY

BASED ON TOTAL SURFACE AREA S_o

REYNOLDS NUMBER : 6×10^5

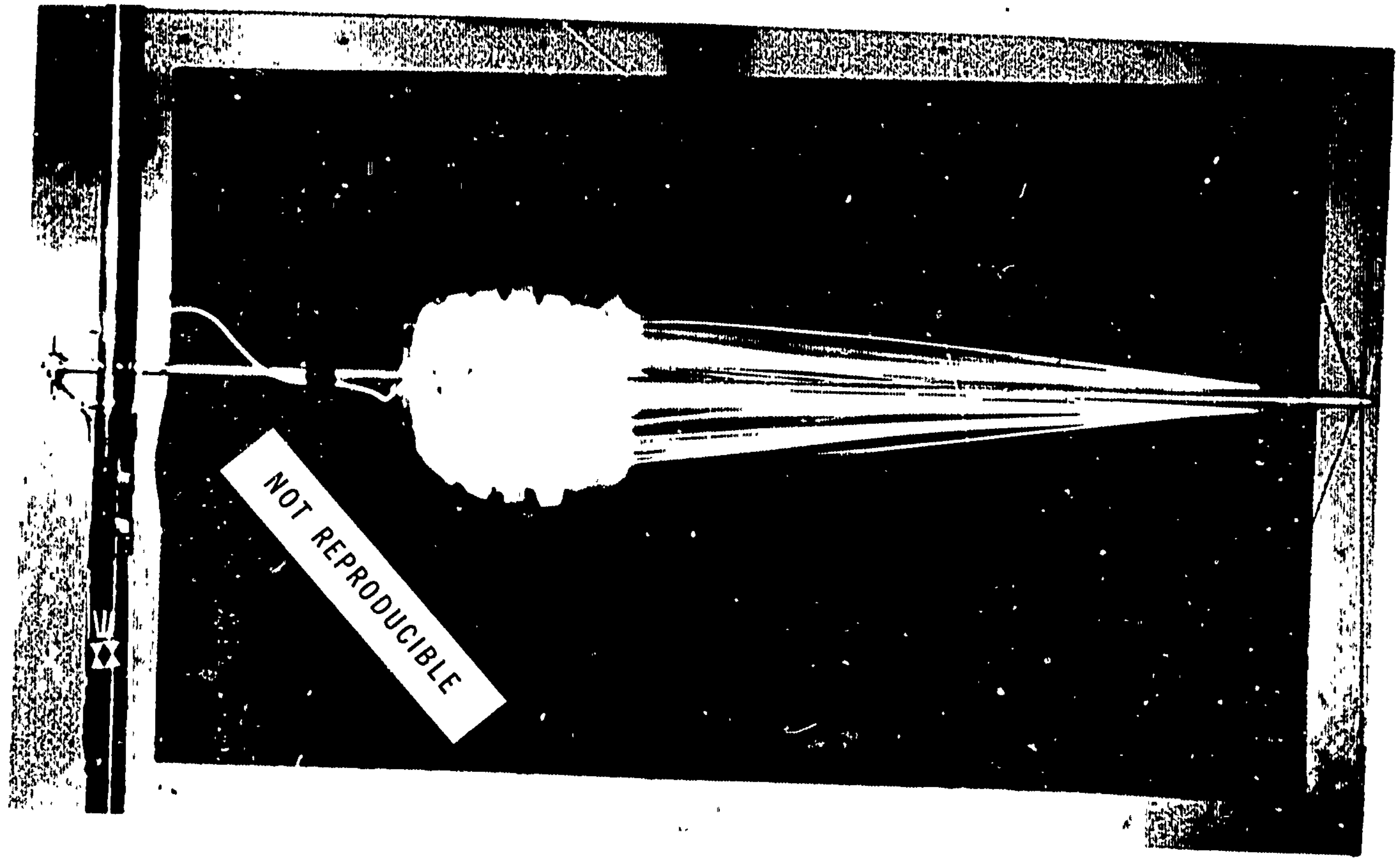

FIG A-12. 50" PROTOTYPE DIAMETER RIBBON PAPACHUTE MODEL OF 30% GEOMETRIC POROSITY IN WIND TUNNEL
REYNOLD'S NO. $\cong 6 \times 10^5$

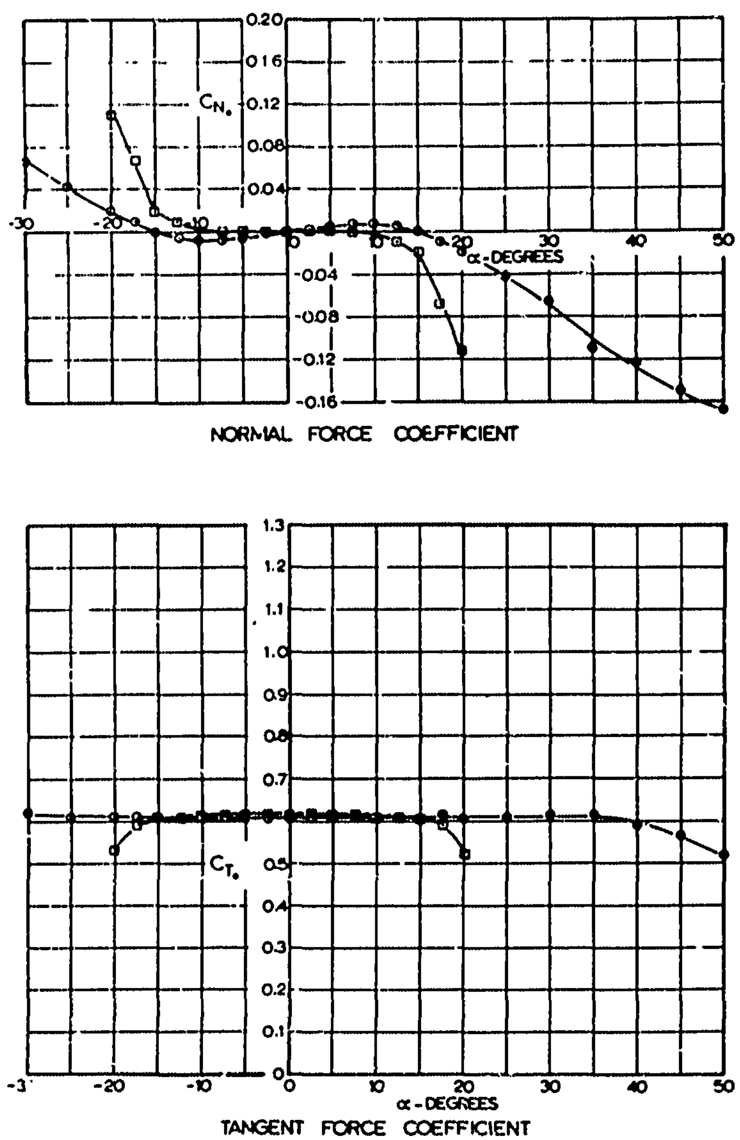

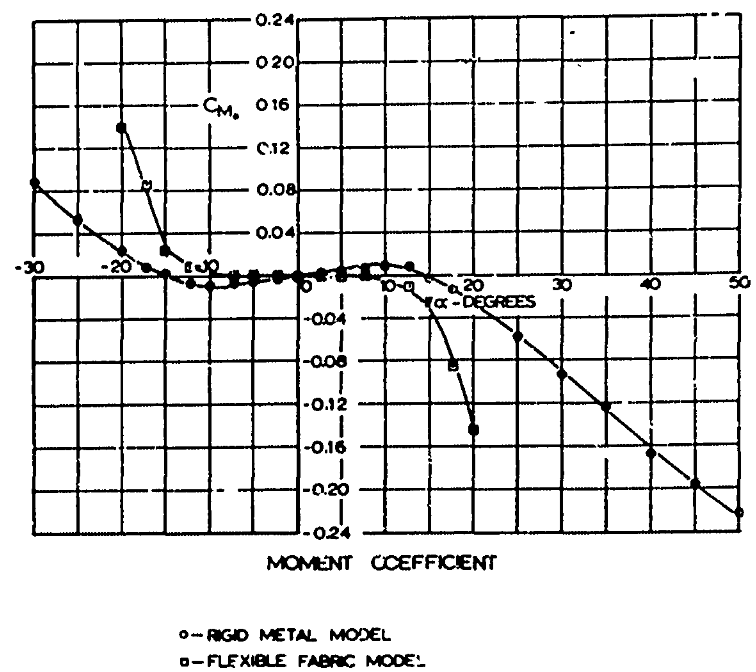

FIG A-13. CHARACTERISTIC COEFFICIENTS VERSUS ANGLE OF ATTACK FOR 50" PROTOTYPE DIAMETER RING SLOT PARACHUTE OF 20% GEOMETRIC POROSITY

BASED ON TOTAL SURFACE AREA S_o, REYNOLDS NUMBER ≅ 6×10^5

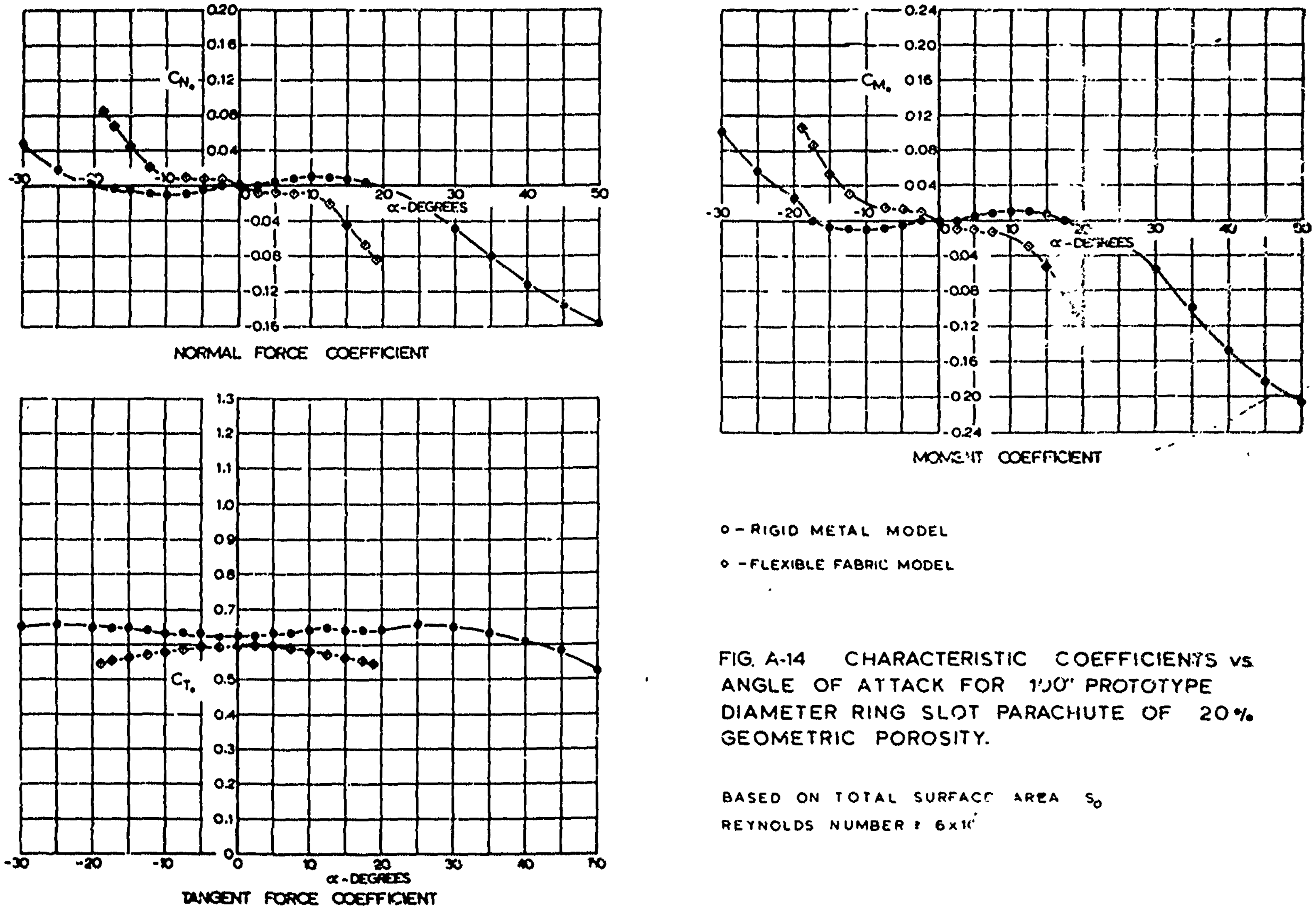

○ – RIGID METAL MODEL

◇ – FLEXIBLE FABRIC MODEL

FIG. A-14 CHARACTERISTIC COEFFICIENTS vs ANGLE OF ATTACK FOR 100' PROTOTYPE DIAMETER RING SLOT PARACHUTE OF 20% GEOMETRIC POROSITY.

BASED ON TOTAL SURFACE AREA S_0

REYNOLDS NUMBER ≈ 6x10

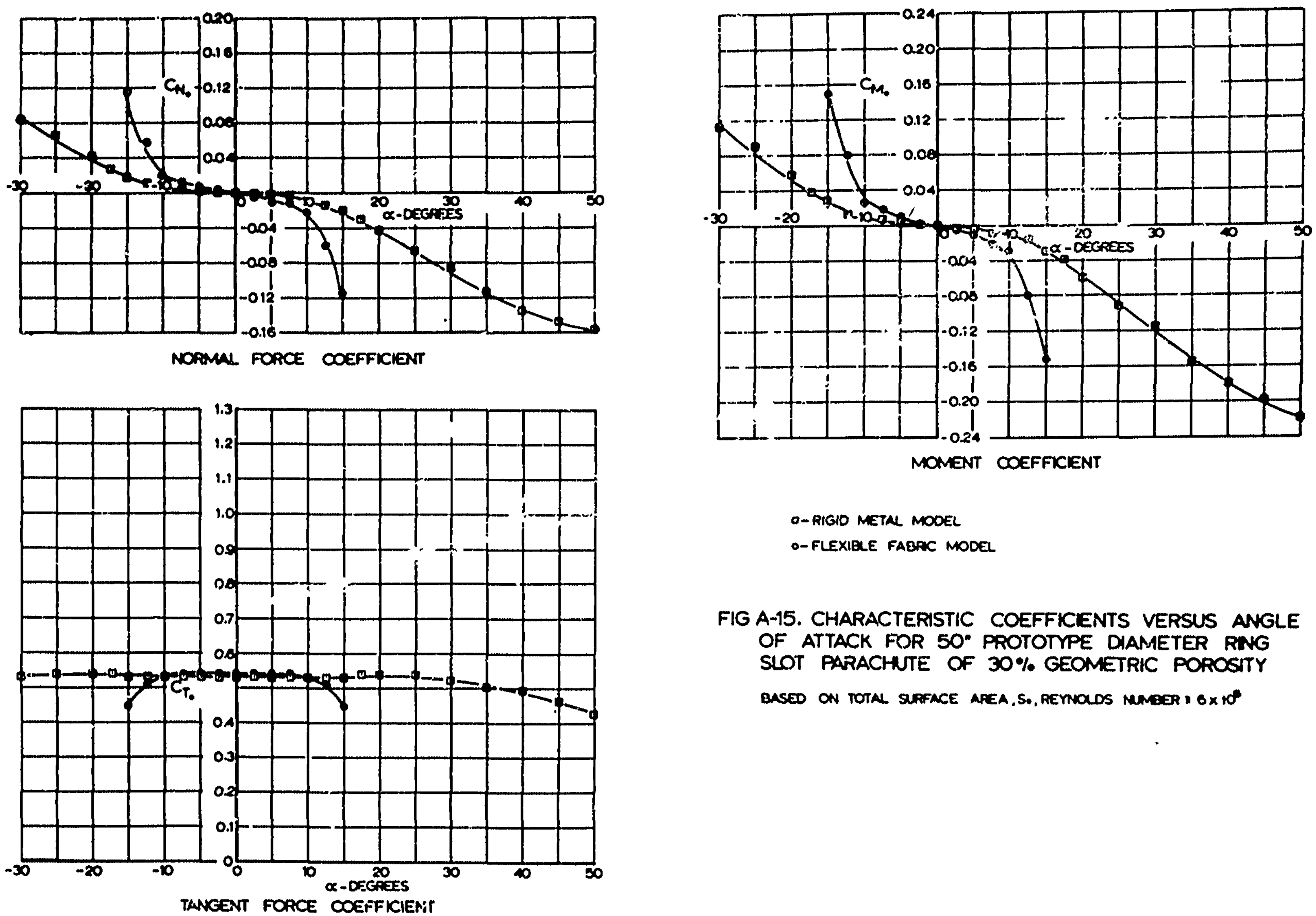

□ – RIGID METAL MODEL
○ – FLEXIBLE FABRIC MODEL

FIG A-15. CHARACTERISTIC COEFFICIENTS VERSUS ANGLE OF ATTACK FOR 50' PROTOTYPE DIAMETER RING SLOT PARACHUTE OF 30% GEOMETRIC POROSITY

BASED ON TOTAL SURFACE AREA, S_o, REYNOLDS NUMBER ≈ 6×10^6

APPENDIX B

DIMENSIONLESS PROFILES OF PARACHUTE CANOPIES

The fabrication of rigid parachute models made from sheet metal required a knowledge of the "in-flight" profile of the various types of parachute canopies. These profiles were obtained from existing data as follows:

1) Photographic gore centerlines of the circular flat, conical, personnel guide surface, and 10% flat extended skirt canopies are found in Ref 4. Reference 8 contains the data for extensions on the personnel guide surface model.
2) Guide surface profiles were obtained from Ref 7, and are presented in Fig B-1 of this appendix.
3) The 14.3% full extended skirt profile was obtained from Ref 2.
4) The ribbon and ring slot canopies used the same profile as the circular flat canopy.

To increase the accuracy in reproducing the metal models from photographic profiles, and to eliminate the need for scaling models from these profiles, dimensionless profile tables were derived for the circular flat, conical, personnel guide surface, 10% flat extended skirt, and the 14.3% full extended skirt canopies. These dimensionless profile tables relate the maximum, or planform radius, x_m, to the x and y components of points on the profile as follows:

1) The maximum radius, x_m, was measured
2) The vertical, or y axis was divided into equi-distant points
3) From these points the horizontal distance to the photographic gore centerline was measured and designated as "x"

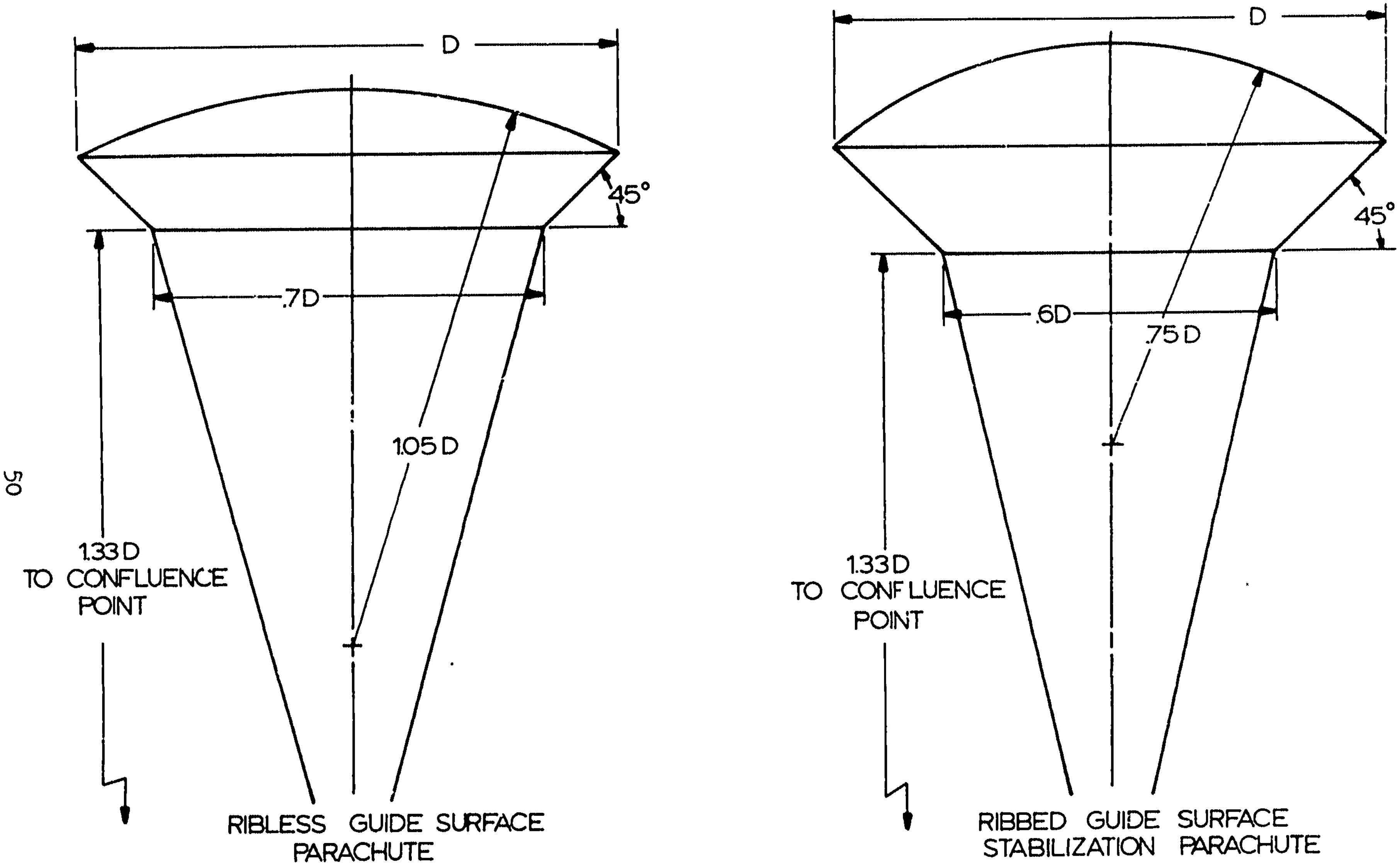

FIG B-1 PROFILES OF GUIDE SURFACE PARACHUTES FOR FORMED METAL MODELS

4) Using the base of the parachute skirt as the zero reference line, a distance "y" up to the y axis and the corresponding "x" were divided by x_m to give the dimensionless ratios y/x_m and x/x_m respectively.

Tables B-1 through B-5 present these dimensionless profile ratios for the canopies listed above. Accompanying each table is a sketch showing the profile of the canopy. These ratios can be used to obtain the photographic gore centerline profile for any desired maximum inflated diameter.

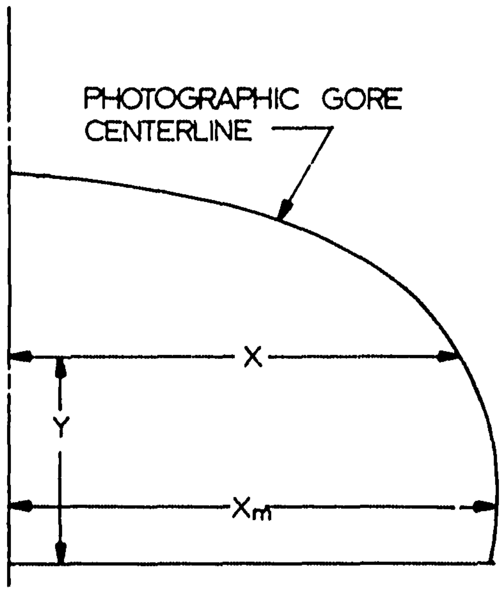

STATION	Y/X_{max}	X/X_{max}
1	0	0.992
2	0.0826	1.0
3	0.162	1.0
4	0.248	0.996
5	0.331	0.975
6	0.413	0.950
7	0.496	0.893
8	0.579	0.818
9	0.661	0.694
10	0.744	0.545
11	0.826	0

TABLE B-1. DIMENSIONLESS PROFILE FOR CIRCULAR FLAT PARACHUTE

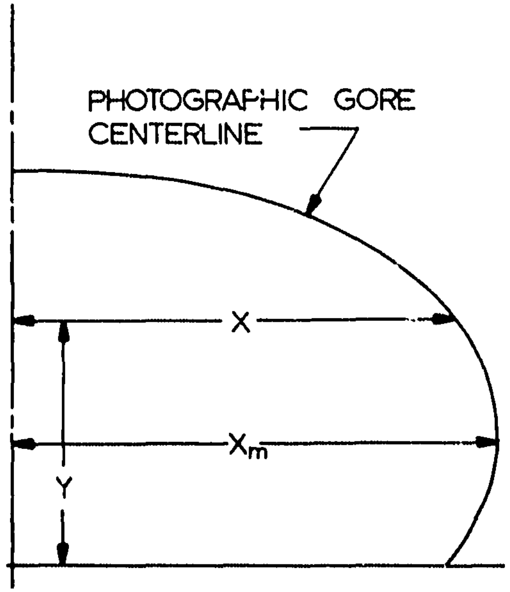

STATION	Y/X_{max}	X/X_{max}
1	0	0.908
2	0.0817	0.958
3	0.163	0.993
4	0.245	1.0
5	0.327	0.993
6	0.408	0.975
7	0.490	0.926
8	0.577	0.859
9	0.654	0.768
10	0.735	0.613
11	0.789	0.458
12	0.817	0

TABLE B-2. DIMENSIONLESS PROFILE FOR 10% FLAT EXTENDED SKIRT PARACHUTE

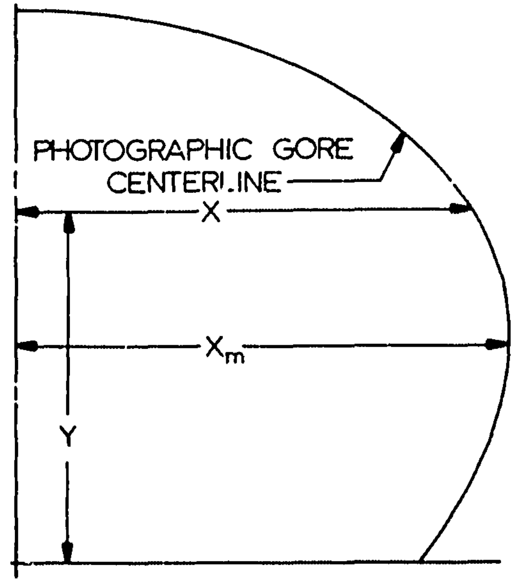

STATION	Y/X_{max}	X/X_{max}
1	0	0.824
2	0.119	0.901
3	0.238	0.967
4	0.356	0.989
5	0.475	1.000
6	0.593	0.967
7	0.712	0.945
8	0.831	0.879
9	0.949	0.736
10	1.068	0.549
11	1.187	0

TABLE B-3. DIMENSIONLESS PROFILE FOR 14.3% FULL EXTENDED SKIRT PARACHUTE

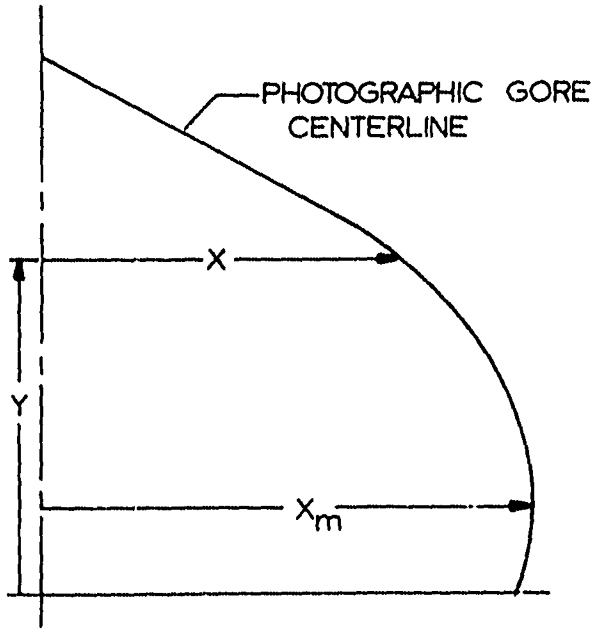

Station	Y/X_{max}	X/X_{max}
1	.0	.964
2	.1136	.984
3	.2272	.991
4	.341	.973
5	.455	.936
6	.568	.868
7	.632	.745
8	.795	.582
9	.91	.377
10	1.02	.182
11	1.15	.0

TABLE B-4. DIMENSIONLESS PROFILE FOR CONICAL PARACHUTE

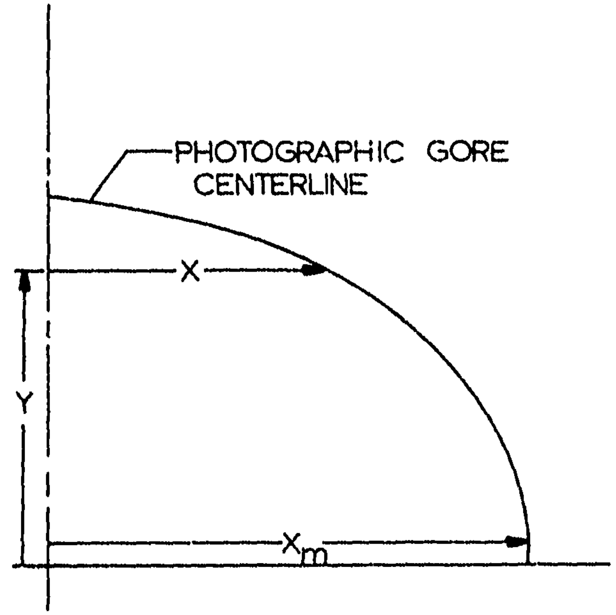

Station	Y/X_{max}	X/X_{max}
1	.0	1.0
2	.078	.992
3	.156	.975
4	.234	.932
5	.312	.898
6	.390	.852
7	.468	.788
8	.546	691
9	.624	.551
10	.707	.407
11	.780	.0

TABLE B-5. DIMENSIONLESS PROFILE FOR PERSONNEL GUIDE SURFACE PARACHUTE

APPENDIX C

EFFECTS OF SUSPENSION LINES ON AERODYNAMIC COEFFICIENTS

As a supplement to the work described in the main body of this report, wind tunnel tests were conducted on a high porosity circular flat parachute model (nominal porosity = 275 ft^3/ft^2-min) to determine the effect of suspension line diameter on the aerodynamic characteristics.

The cloth parachute models, as received from the manufacturer, were fitted with 0.096 inch diameter suspension lines, as compared to a true scale diameter of 0.006 inch. Since this is a rather large departure from scale size, it was considered necessary to determine the errors introduced in the data due to the increased drag area and wake turbulence of the thicker suspension lines.

To determine the effects of the larger suspension lines, two consecutive test series were conducted on the circular flat canopy, first with 0.096 inch diameter suspension lines, and then with these lines replaced by 0.020 inch diameter lines. The results of these tests are shown in Fig C-1. We see that the tangent force coefficients are reduced by less than 2% when the thinner lines are used. Similarly, the error introduced in values of the normal force and moment coefficients is less than 1%.

The small errors caused by the larger suspension lines were deemed negligible, and all further tests were conducted with the models as received from the manufacturer (i.e., with 0.096 inch diameter suspension lines).

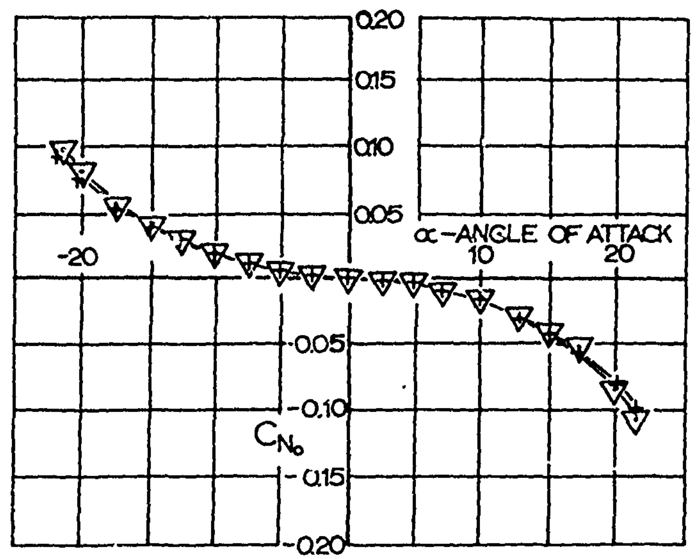

NORMAL FORCE COEFFICIENTS

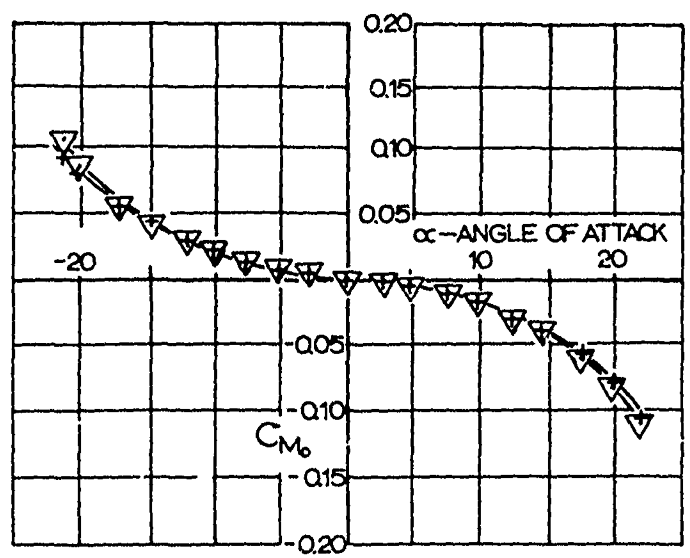

MOMENT COEFFICIENTS

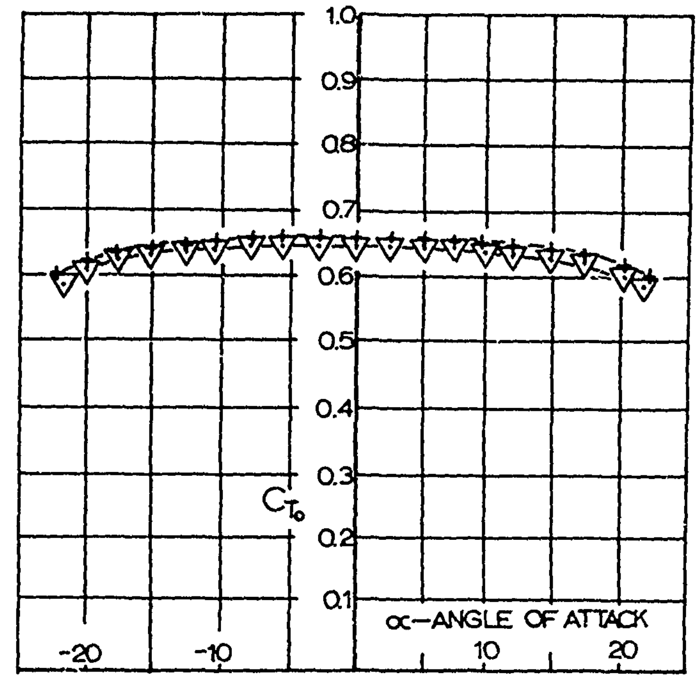

TANGENT FORCE COEFFICIENTS

KEY

SYMBOL	SUSPENSION LINE DIAMETER
+	0.096 INCH
▽	0.020 INCH

FIG. C-1. EFFECT OF SUSPENSION LINE DIAMETER ON CHARACTERISTIC COEFFICIENTS OF A CIRCULAR FLAT PARACHUTE MODEL

BASED ON TOTAL CLOTH AREA
NOMINAL CLOTH POROSITY = 275 FT^3/FT^2–MIN.
REYNOLDS NUMBER = 6×10^5

APPENDIX D

DEVELOPMENT OF THE PARACHUTE BALANCE SYSTEM

For several reasons it was decided to develop a balance system which could be used for all types of parachutes and in which the forces would be measured by strain gage elements in connection with a recording oscillograph. Figure D-1 illustrates the general arrangement; it is seen that the parachute is supported by a sting which is held in a horizontal position by means of suspension wires and a strut mounted to two turntables. The tangential force of the parachute activates the drag link mounted ahead of the parachute canopy which served at the same time as the confluence point of all suspension lines. The normal force can be picked up at a strain gage sensing element fastened to the apex of the parachute canopy. The drag link is rigidly fastened to the front suspension point while the strain gage link which measures the normal force rides on the canopy with a minimum of friction on the center sting. The normal force sensing element is shown in the main body of this report in Fig 5.

With an arrangement of this nature, a number of these component measurements were carried out, and Fig D-2 illustrates a resultant normal force curve versus angle of attack. We see that the normal force is somewhat affected by the upstream disturbance of the drag link as well as by the center sting. In order to investigate the effect of this suspension system, the entire arrangement was changed to a configuration as shown in Fig D-3. It can be seen that in this arrangement the center sting is removed and the canopy is held in position by a rear sting. Measurements with this arrangement show a noticeable difference as a comparison between the Figs D-2 and D-4 indicates.

The upstream tangential force sensing element was of considerable size and to investigate whether the size of this center obstruction would influence the measurement

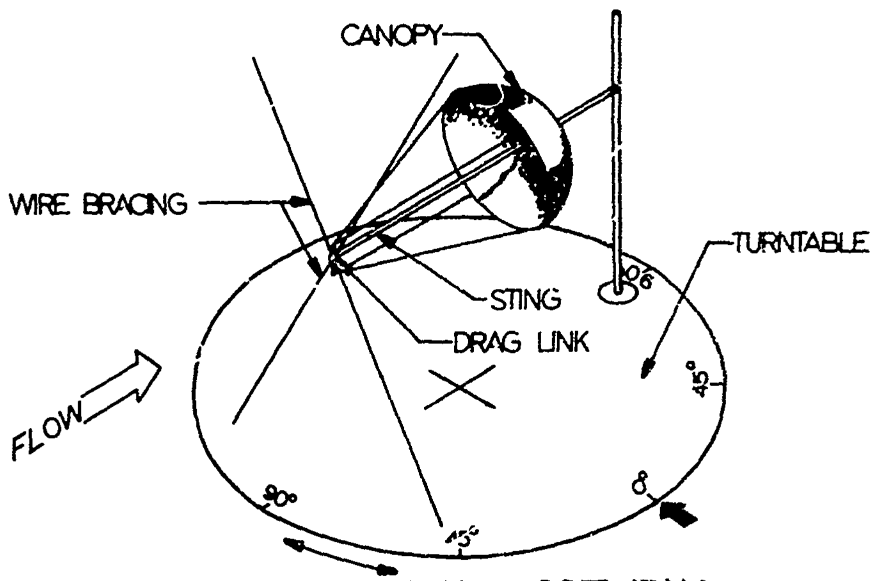

FIG D-1. TEST SECTION ASSEMBLY WITH STING AND DRAG LINK

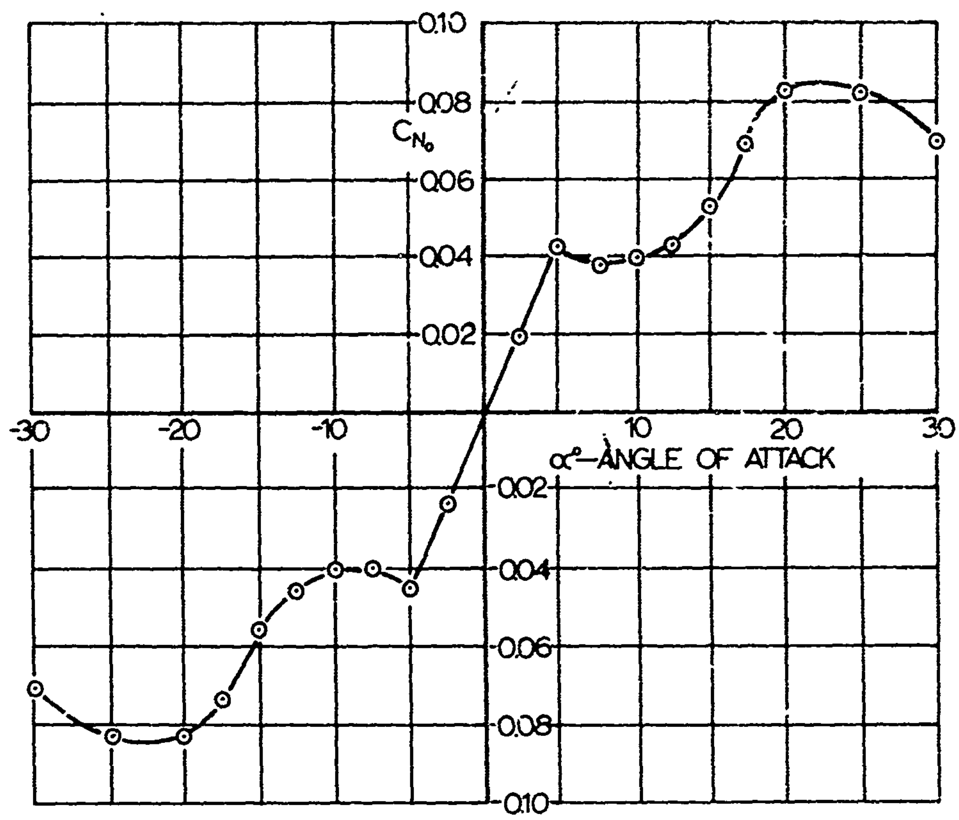

FIG D-2. NORMAL FORCE COEFFICIENT VERSUS ANGLE OF ATTACK FOR CIRCULAR FLAT PARACHUTE (WITH STING AND DRAG LINK)

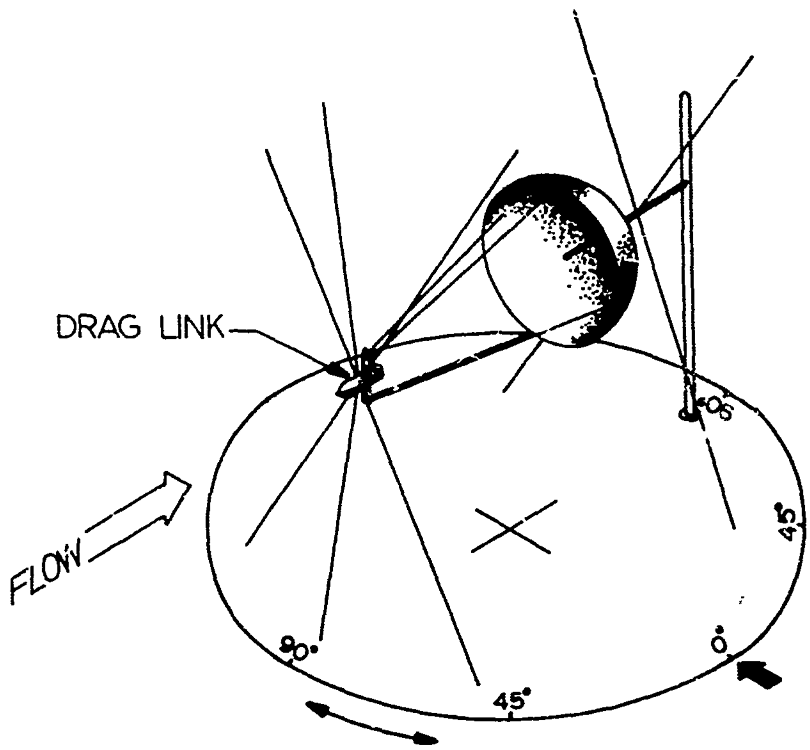

FIG D-3. TEST SECTION ASSEMBLY WITH DRAG LINK, NO STING

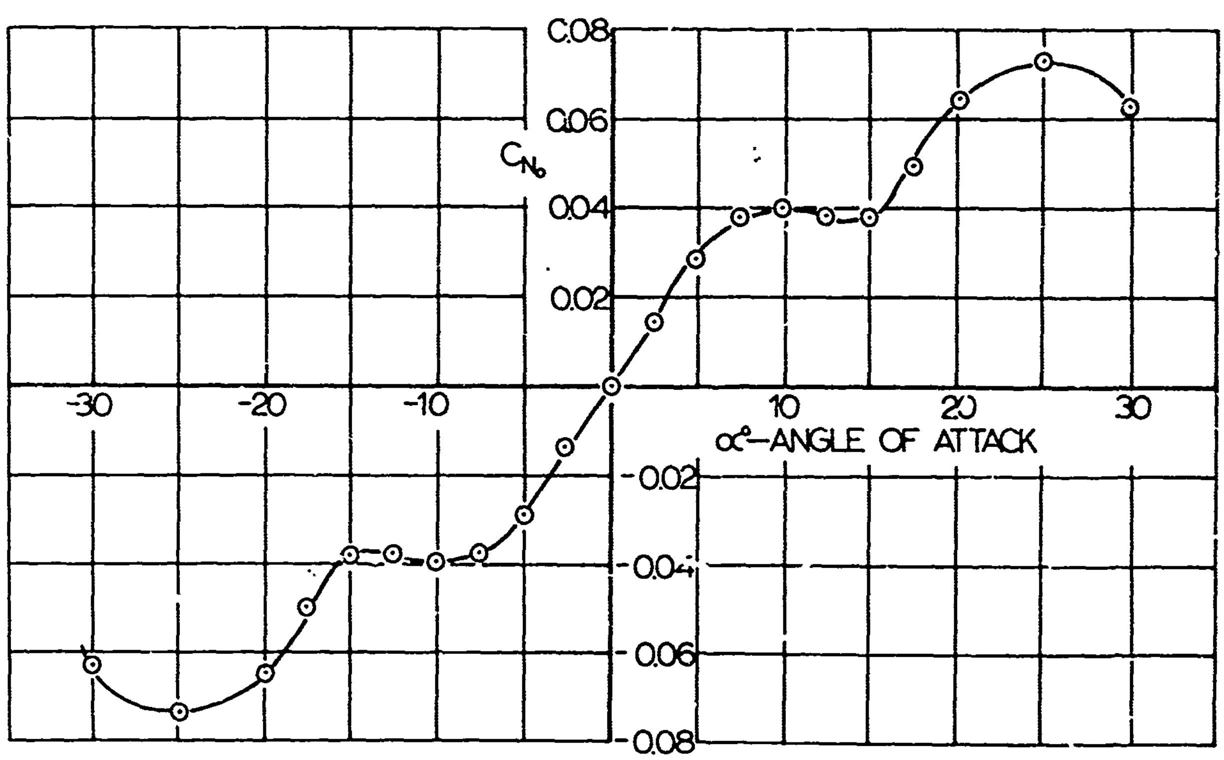

FIG D-4. NORMAL FORCE COEFFICIENT VERSUS ANGLE OF ATTACK FOR CIRCULAR FLAT PARACHUTE MODEL (DRAG LINK ONLY) significantly, the arrangement was further modified to a configuration as shown in Fig D-5. In this suspension system the center obstruction is reduced to a somewhat streamlined body of minimum size and the long center sting is completely removed. Measurements with this arrangement provided a characteristic normal force curve as shown in D-6. Since in this configuration the suspension of the model includes a minimum of obstructions, one may consider that this suspension would be the most ideal to obtain the aerodynamic characteristics of a parachute canopy with suspension lines running together in one confluence point. However, such an arrangement is somewhat impractical since it is very difficult to arrange the center of the parachute canopy perfectly in line with a confluence point and the direction of air flow. Furthermore, this arrangement would not provide the possibility of measuring any tangential force. Therefore, the arrangement of a thin center sting would be highly desirable, and Fig D-7 indicates this modified suspension system.

Measurements with this more practical arrangement were carried out and a characteristic curve of normal forces versus angle of attack is shown in D-8. A comparison between Figs D-6 and D-8 indicates a certain deviation in the normal force, obviously caused by the introduction of the center sting. However, this arrangement would offer the possibility of measuring tangential as well as normal forces and would also assure a proper alignment of the parachute model with the direction of flow.

After these preliminary examinations, a new suspension system was designed which is illustrated in Figs 3 and 4 of the main body of this report. In this configuration the parachute model is centered by a very thin sting which can slide with the minimum of friction in the front suspension supporting point. The apex of the canopy rests on the center sting by means of the normal force pickup which is secured against rotation by means of a keyway and slot. The sting rests at its rearward end on the tangent force measuring

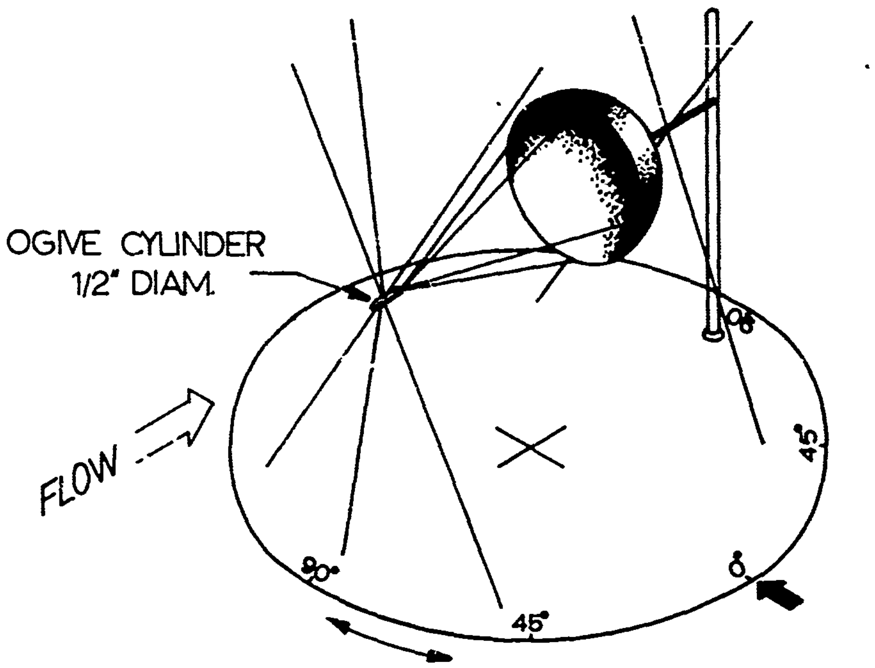

FIG D-5. TEST SECTION ASSEMBLY WITH NO STING, NO DRAG LINK

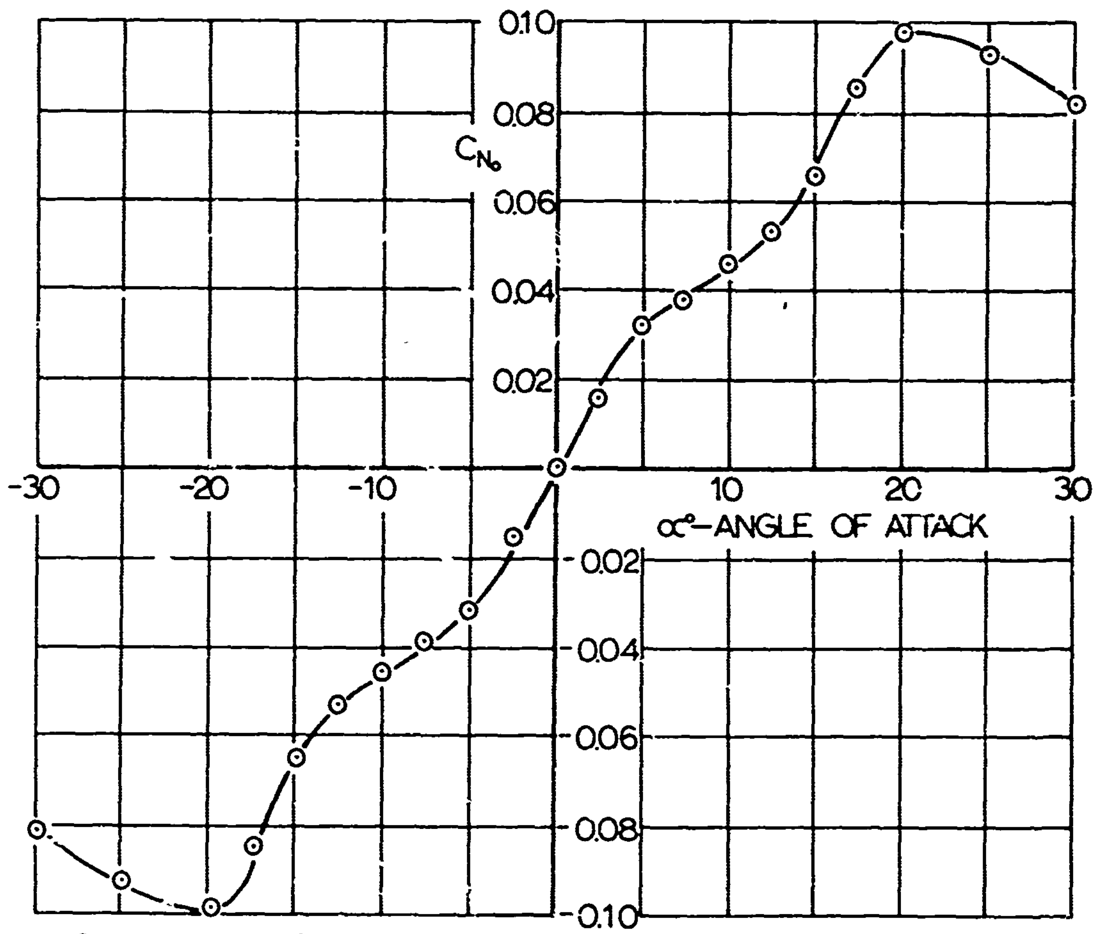

FIG D-6. NORMAL FORCE COEFFICIENT VERSUS ANGLE OF ATTACK FOR CIRCULAR FLAT PARACHUTE MODEL (NO STING, NO DRAG LINK)

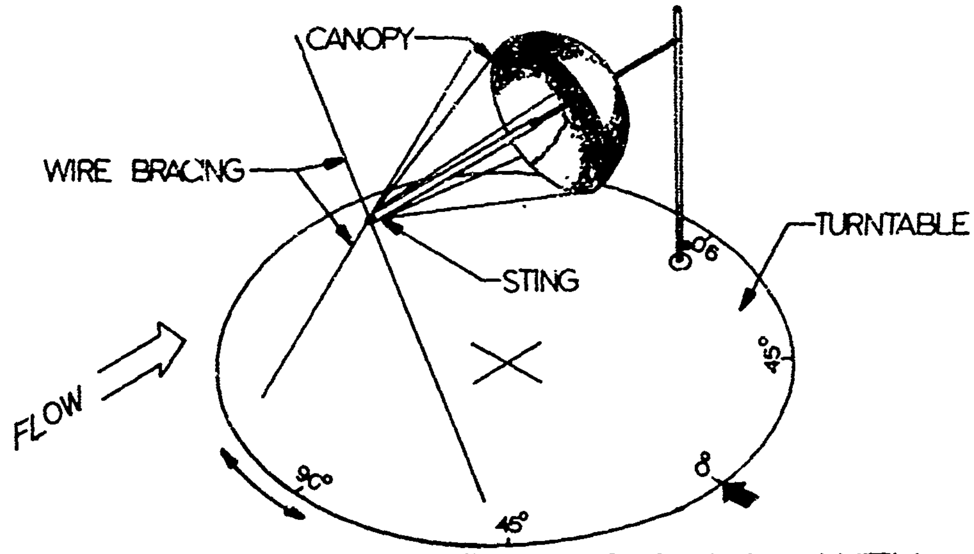

FIG D-7. TEST SECTION ASSEMBLY WITH STING ONLY, NO DRAG LINK

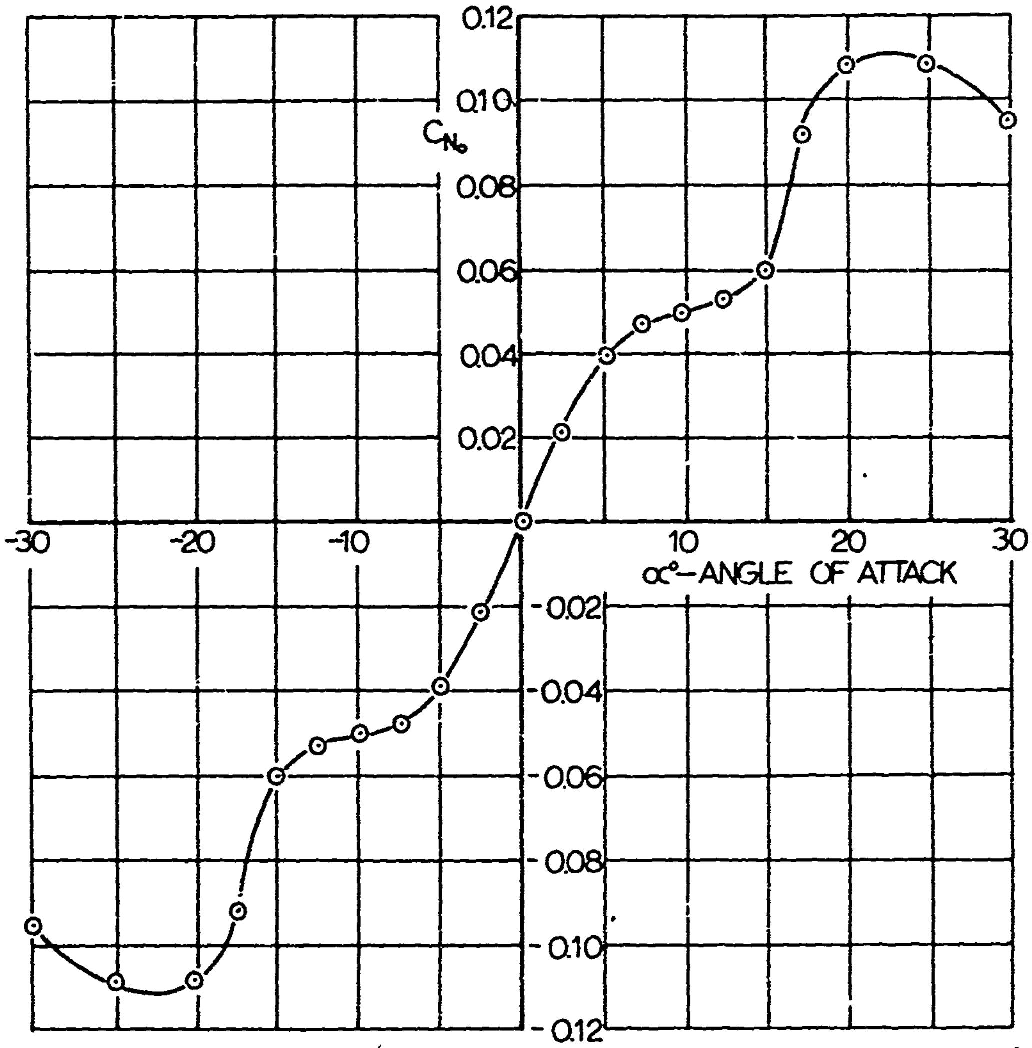

FIG D-8. NORMAL FORCE COEFFICIENT VERSUS ANGLE OF ATTACK FOR CIRCULAR FLAT PARACHUTE (WITH STING ONLY, NO DRAG LINK) element. To prevent excessive side movement, which has to be expected particularly from unstable parachutes, the rear vertical strut is provided with a bearing support which assures a minimum of friction if contact between strut and center sting occurs. It can be seen that in this arrangement all supporting elements were made as small as possible. Measurements with this arrangement were carried out and the normal force curve is shown in Fig D-9. A comparison of Fig D-9 and Fig D-6 indicates that this new normal force curve deviates very slightly from the curve which had been established as the ideal curve for force measurements.

In view of the results of this investigation, the balance system as illustrated in Figs 3 and 4 was made the standard system and has been used for the establishment of all aerodynamic data shown in this report.

It is worthwhile to mention that the difference in the method of measurement and model suspension was most strongly noticeable in the normal force curves. The effects of the upstream disturbances and the center sting were hardly noticeable in the tangential force measurements and were practically so small that reliable measurements of the differences were impossible.

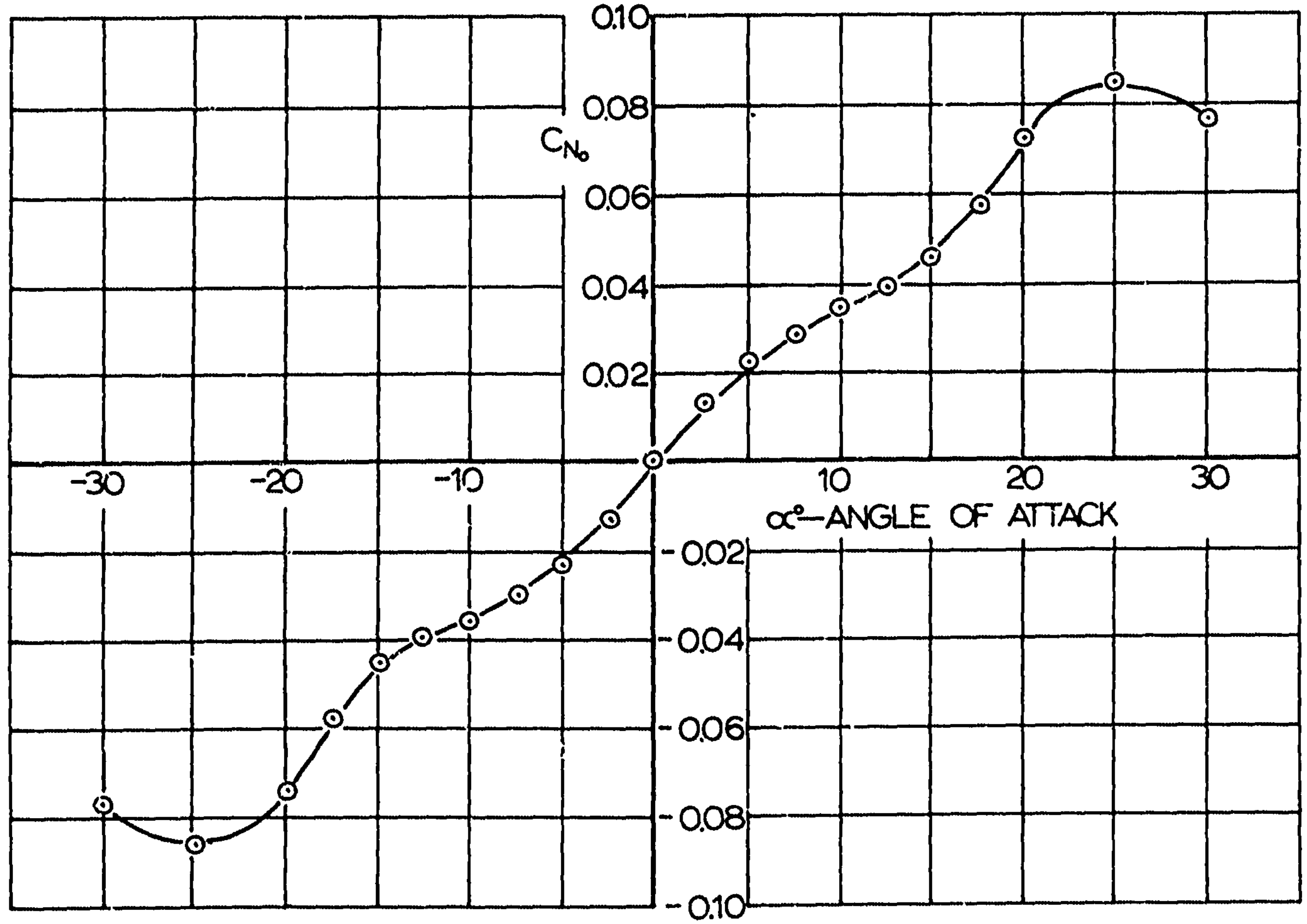

FIG D-9. NORMAL FORCE COEFFICIENT VERSUS ANGLE OF ATTACK FOR CIRCULAR FLAT PARACHUTE MODEL (WITH FINAL TEST ARRANGEMENT)

★ U. S. Government Printing Office: 1971 – 759-076/007